DETECTION OF SLEEP AND WAKE SUBSTATES THROUGH UNSUPERVISED MACHINE LEARNING IN RAT HIPPOCAMPUS AND PRIMARY MOTOR CORTEX LFP RECORDINGS

PAULINE BALOGUN
Bachelor of Science, University of Alberta, 2014

A Thesis
Submitted to the School of Graduate Studies
Of the University of Lethbridge
In Partial Fulfillment of the
Requirements for the Degree of

MASTER OF SCIENCE

in

NEUROSCIENCE

Department of Neuroscience
University of Lethbridge
LETHBRIDGE, ALBERTA, CANADA

DETECTION OF SLEEP AND WAKE SUBSTATES THROUGH UNSUPERVISED MACHINE LEARNING IN RAT HIPPOCAMPUS AND PRIMARY MOTOR CORTEX LFP RECORDINGS

PAULINE BALOGUN

Date of Defence: December 17, 2019

Dr. M. Tatsuno Supervisor	Associate Professor	Ph.D.
Dr. B. McNaughton Thesis Examination Committee Member	Professor	Ph.D.
Dr. D. Euston Thesis Examination Committee Member	Associate Professor	Ph.D.
Dr. A. Luczak Thesis Examination Committee Member	Professor	Ph.D.
Dr. A. Iwaniuk Chair, Thesis Examination Committee	Associate Professor	Ph.D.

DEDICATION

This is dedicated to my mother who passed before she could see her dream come true and to my husband who supported me through it all. This is thanks to you.

ABSTRACT

This project investigated whether unsupervised machine learning could detect differences in global or local microstates across different rodent brain, in the effects of procedural learning, and clustering validity indices effectiveness. Previously obtained local field potential recordings of M1 and the hippocampus of freely-behaving male rats under naïve and task conditions, including transcranial direct and alternating current stimulation (tDCS; tACS), were analyzed and used to assess several methods. Two local SWS-like REM microstates were detected along with five global microstates. Learning suppressed cortical SWS-like REM microstates, but tDCS negated this effect. Calinski-Harabasz evaluated clusters had the highest sensitivity, specificity and total accuracy. Local and global brain states were effectively detected using PCA and clustering, and measures of phase-amplitude coupling were sensitive to the task conditions. These changes could underlie consolidation windows for procedural learning with potential intervention by tDCS although these results are limited to due the quality of the dataset.

ACKNOWLEDGEMENT

I would like to thank my supervisor, Dr. Masami Tatsuno for his support and guidance during my graduate work. Thank you to my committee members, Dr. Bruce McNaughton, Dr. David Euston and Dr. Artur Luczak, for sitting on my thesis committee and providing me support throughout my graduate work. Thank you to the members of the Tatsuno lab, past and present, without whom I never would have finished my project

I must extend a special thanks to Kartik Iyer, Karim Ali and Michael Eckert for giving me so much of their time to show me the ropes and answering my constant questions. Thank you to all my fellow graduate students at CCBN who provided a listening ear and a cup of something warm throughout my journey here.

Thank you to my husband, my family and my friends who motivated me to keep going and encouraging to follow my dreams.

TABLE OF CONTENTS

LIST OF TABLES

LIST OF FIGURES

LIST OF ABBREVIATIONS

AAC	Amplitude-Amplitude Coupling
AC	Alternating Current
BD	Baseline Day
BM	Body Movement
CFC	Cross-Frequency Coupling
CH	Calinski-Harabasz
coh	Coherence
CPSD	Cross Power Spectral Density
CSD	Current Source Density
CTX	Cortex
CVI	Cluster Validity Index
DB	Davies-Bouldin
DC	Direct Current
EEG	Electroencephalogy
EMG	Electromyography
f_A	Frequency for Amplitude
f_P	Frequency for Phase
G	Grooming
HIP	Hippocampus
HS	Head Shift
Hz	Hertz
I	Current
IRtPAC	Inter-Regional time-resolved Phase-Amplitude Coupling
LFP	Local Field Potential
M	Motionless
M1	Primary motor cortex
MVL	Mean Vector Length
NREM	Non-Rapid Eye Movement
PAC	Phase-Amplitude Coupling
POST-A	Post-Task tACS
POST-D	Post-Task tDCS
PPC	Phase-Phase Coupling
PRE-A	Pre-Task tACS
PRE-D	Pre-Task tACS
pREM	phasic Rapid Eye Movement
PS	Paradoxical Sleep
PSD	Power Spectral Density
PLV	Phase-Locking Value
R	Resistance
r	Correlation
REM	Rapid Eye Movement
RR	Respiration-entrained oscillations
SEM	Standard Error of the Mean
SF	Sniffing/whisking

SH	Silhouette
S-PRE	Sham Pre-Task
S-POST	Sham Post-Task
S-SIA	Sleep Small-amplitude Irregular Activity
SWR	Shape Wave Ripple
SWS	Slow Wave Sleep
TAC	Total Accuracy
tACS	Transcranial Alternating Current Stimulation
TD	Task Day
tDCS	Transcranial Direct Current Stimulation
tPAC	Time-resolved Phase-Amplitude Coupling
tREM	Tonic Rapid Eye Movement
MSC	Magnitude-Squared Coherence
V	Voltage
mV	Millivolt
n.s.	Not Significant

1. General Introduction

It should be emphasized that this project is a methodological one that explores the detection capabilities of a sample dataset.

First, this paper will establish the definitions of key terms in this paper as a number of them have various meanings throughout the literature.

Perhaps the most fundamental definition is that of an oscillation - a repetitive displacement, especially in time, around a central value. A swinging pendulum is an example of a spatial oscillation. This paper concerns itself with electrical brain oscillations. These are generated by the repetitive firing a neuron or neurons, depending on scale and can be generated by either spatially and/or temporally connected neurons (Cole & Voytek, 2017). For LFP recordings, it is assumed that the dipole generated by the movement of charges in and out of firing neurons is spatially limited to only one or a few proximal neurons although other signals may be present and should be accounted for (Kajikawa & Schroeder, 2011).

Brain oscillations form the foundation for the level of consciousness, or brain state, exhibited by an organism. These can be broader such as awake, asleep or comatose or more specific like alert or drowsy. This project focuses on three brain states: awake, in REM sleep or in non-REM sleep. It was generally held that these states were global i.e. the entirety of the brain could only be in one state at a time such that if an organism was in REM sleep, all brain regions would exhibit REM sleep characteristics. Recently, research supports the presence of local states where the majority of the brain will be in one state while a minority of regions will exhibit traits of another (D'Ambrosio et al., 2019). There is even a medical disorder where parts of the brain enter a sleep state while

the individual is still awake (Vyazovskiy et al., 2011).

In addition to the occurrence of local states during global ones are finer divisions within brain states, particularly sleep states. In humans, the most recognizable of these are the stages of sleep, which humans cycle through during a regular night's sleep. The stages have distinct traits that are evident not just in the brain, but throughout the body. In animals these stages have not been as definitively established with only REM and NREM, usually called slow wave sleep, being the only consistent divisions. However, there is emerging evidence that SWS and even REM in both humans and animals may be more finely divided into microstates. The theory is that there may be consistent periods within brain states that underlie specific brain activity and functions.

One such function is consolidation although it may be more accurate to consider this a category of related functions. Consolidation is a complex series of processes that begins within minutes and hours of acquisition and can continue for years and even decades in some species (McGaugh, 2000). It can be broken down into synaptic consolidation, which occurs following acquisition and creates a memory which persists for 24 hours (Clopath, 2012). From there, systems consolidation creates a persistent memory with a transfer from the hippocampus to the cortex. Systems consolidation is multifaceted with numerous theories as to the precise mechanisms governing the many types of memories and brain regions involved (Antony & Schapiro, 2019). For instance, the amygdala, especially the basolateral nuclei, is heavily involved in emotional memory consolidation and plays a significant role in fear conditioning (Beckers & Kindt, 2017). There are also differences in consolidation and retrieval of declarative and procedural memories. An oft-cited reason for this is because amnesiac patients (individuals lacking

declarative memory) can learn and retain novel procedural tasks, the process of consolidation between the two types of memory must also be separate (Quillfeldt, 2019). Finally, there's also re-consolidation, a hotly debated phenomenon whereby consolidated memories are retrieved and consolidated again (Beckers & Kindt, 2017). It's been proposed as a mechanism for modifying existing memories and as a tool in psychotherapeutic practice.

1.1 Unsupervised Machine Learning

Machine learning is a subset of artificial intelligence that refers to the algorithms and models that information processors use to perform tasks while relying on patterns and inference (Lloyd et al., 2013; Bishop, 2006). Machine learning can be further divided into three categories: supervised, unsupervised, and reinforcement learning. In supervised learning, the algorithm is given training data, sample data that contains known input and matching output data. For example, a publisher wants to know when households cancel their subscriptions. They have the subscription history of 10,000 households, 5,000 cancelled and 5,000 still subscribed. The data of 4,000 cancellation households and 4,000 subscribed households is given to the model. The model is then used to predict the subscription status of the excluded households, which can then be compared against the real subscription status to calculate the accuracy of the model. Adjustments are then made in order to minimize the differences between the known output and the one generated by the algorithm and increasing the accuracy. In unsupervised learning, there is no training data set and the algorithm uses the characteristics in the data to find similarities and differences to form clusters of like data. Reinforcement learning generally involves a rule or condition set that the algorithm follows to achieve a goal with penalties and rewards

assigned for failures and successes in a dynamic environment (Lloyd et al., 2013). In other words, the algorithm monitors the response to the actions taken and measures that against a defined reward or penalty in order to judge the quality of its performance. The quality of a run can be considered good or bad with the algorithm adjusting subsequent runs to improve the quality by using fewer moves, getting faster completion times, etc. Board games and video games are popular environments for these algorithms. For this study, unsupervised learning is used to find brain states and substates using an unlabelled EEG data set. The unsupervised learning paradigm uses the k-means clustering algorithm as it is relatively popular, accessible and is relatively insensitive to noise although it can be slower than other algorithms i.e. require a higher number of iterations and may occasionally fail to differentiate between small and large clusters near close together (Arbelaitz et al., 2013; Hämäläinen et al., 2017).

Fundamentally, clustering is a method of grouping observations together based on how similar they are to each other. Similarity can be defined as a measure of closeness, often called distance. Physical distance is a positive value defining two points in relation to each other. For example, Hawaii is 6,600 kilometres from Japan and Japan is 6,600 km from Hawaii, but it could not be said that Hawaii is -6,600 km from Japan. The mathematical distance between data points is relative to zero, so any point can have a negative distance. When comparing the distance between points, having opposing signs would negate the effect. So clustering algorithms implement a variety of distance measurements that prevent summing positive and negative values together. One of the most common is squared Euclidean distance, which is used in this study and is passed to the k-means algorithm. The k-means algorithm, originally published by Lloyd (1982) and

then later refined as k-means++ (Arthur & Vassilvitskii, 2007), begins with a randomly selected data point being used as the centre of the first cluster, assuming a k number of clusters. The steps for k-means++ are as follows:

1) Select an observation uniformly at random from the data set, X. The chosen observation is the first centroid, and is denoted c_1.
2) Compute distances from each observation to c_1. Denote the distance between c_j and the observation m as $d(x_m, c_j)$.
3) Select the next centroid, c_2 at random from X with probability

(1)

$$\frac{d^2(x_m, c_1)}{\sum_{j=1}^{n} d^2(x_j, c_1)}$$

4) To choose center j:
    a) Compute the distances from each observation to each centroid, and assign each observation to its closest centroid.
    b) For $m = 1,...,n$ and $p = 1,...,j-1$, select centroid j at random from X with probability

(2)

$$\frac{d^2(x_m, c_p)}{\sum_{\{h;\, x_h \in C_p\}} d^2(x_h, c_p)}$$

where C_p is the set of all observations closest to centroid c_p and x_m belongs to C_p.

That is, select each subsequent center with a probability proportional to the distance from itself to the closest center that you already chose.

5) Repeat step 4 until *k* centroids are chosen.

There are two key weaknesses of the original algorithm: lengthy running time i.e. high number of iterations before convergence, and arbitrarily poor initialization leading to a poor clustering result. These shortcomings were improved upon in the k-means++ algorithm, increasing the speed (lower number of iterations to convergence) and accuracy (improved initialization; Arthur & Vassilvitskii, 2007).

A key component of the k-means algorithm is selection of a *k* number of clusters. The selection of k can be done in a number of ways, the most common being the use of a cluster validity index (CVI; Kaufmann & Rousseeuw, 1990). CVIs establish a rule that selects the optimal assignment of data points to *k* clusters. Just as there are different ways of defining distance, there are different ways to value different distances. The optimal separation of data points and clusters varies with the type and purpose of a dataset. Thus, CVI can be selected to maximise distances between clusters or minimize distances between points within a cluster or a number of other criteria as needed.

There are dozens of indices for k-means clustering including Dunn, Gamma, C, negentropy increment, Sym, and COP to name a few. A review by Arbelaitz et al. (2013) offers a comprehensive examination of these indices. A key finding of that review was that CVIs could be grouped into three tiers, with the CVIs in the first tier having the most optimal performance overall and those in the third having the poorest. Each tier was significantly different from the other tiers, but CVIs within a tier had little or no statistical

differences between them. Within a tier, CVI performance varied in regard to specific data characteristics such as type and amount of noise, cluster density and degree of overlap, but no single CVI performed well with all data types. For the purposes of this study, three first tier CVIs were selected and compared: Silhouette (SH), Davies-Bouldin (DB) and Calinski-Harabasz (CH).

The **first aim of this study is to determine the relative effectiveness of the three similar CVIs and the suitability of k-means clustering for the detection of states and microstates**.

1.2 Brain State Characteristics

Neuronal oscillations, or brainwaves, which are produced by spike trains, local-field potentials (LFP) or synchronous neuronal ensemble oscillations, form the foundation for fundamental cognitive functions such as perception, motor control, memory and information transfer (Başar et al., 2001; Buzsáki & Draguhn, 2004; Fries, 2005). LFP is the transient electric potential of the extracellular space, typically of spatially and/or temporally summed neurons, generated by changes in the concentration of ions immediately outside the cell or cells in question as a result of cellular electrical activity (Buzsáki et al., 2012). These oscillations, which are observable at every level of the nervous system, can be detected through electroencephalography (EEG) and characterised by their frequency in Hertz (Hz), amplitude in millivolts (mV), and phase in degrees or radians. Recent advances in modelling techniques and ever improving EEG resolution has allowed for even spike train oscillations to be detected by EEG (Haumann et al., 2019). EEG recordings can be invasive or non-invasive, low-density or high-density, but conventionally refers to non-invasive, scalp-recordings with lower resolution

than LFP which is also called micro-, depth or intracranial EEG (Buzsáki et al., 2012). Frequencies are grouped into EEG bands, or ranges, in order of lowest to highest frequency: delta, theta, alpha, beta and gamma.

The precise frequencies involved vary and some bands can further divided such as beta into beta one (12-15 Hz), beta two (15-20 Hz) and beta three (18-40 Hz) in humans (Abhang et al., 2016). They can be further characterised by the cortical and subcortical structures that produce or propagate them. For example, the cholinergic alpha band is generated by the thalamic pacemaker cells and propagated to the occipital lobe (Li et al., 2017). Thus, EEG bands not only serve as electrical landmarks useful for targeting specific brain structures, but those same structures can also be used as a reliable source for studying these bands. Furthermore, frequency bands also form tight associations with specific brain states related to cognitive functions; such as the frontal midline theta band, which often presents during activation of the hippocampus, insula and superior temporal areas among others (Li et al., 2017; Käthner et al., 2014). In humans, theta increases with mental workloads and is associated with problem-solving, self-monitoring, impulse inhibition, working memory, and other encoding processes (Gevins et al., 1998; Gundel & Wilson, 1992; Holm et al., 2009; Mecklinger et al., 1992). Thus, patterns of neuronal activity can be said to have functional relevance characterised by both frequency and location.

The general waking brain state is characterised by low-amplitude, desynchronous alpha, beta, and gamma activity in the cortex while the waking activity of subcortical structures varies by species (Britton et al., 2016). Different cognitive functions and levels of alertness occurring during waking periods are often linked with specific EEG bands in

a specific brain region (Hinterberger et al., 2014). For example, the cholinergic alpha waves predominate in the occipital lobes during wakeful relaxation especially in the dominant hemisphere (Roohi-Azizi et al., 2017).

The sleeping brain is divided into two general states: rapid eye movement (REM) sleep and non-rapid eye movement (NREM) sleep, often called slow wave sleep (SWS) in animals. In humans, NREM is divided into N1, N2, N3 and N4, with N3 and N4 commonly grouped together as one deep sleep stage (Harvard University, 2008). A resource from the Division of Sleep Medicine at Harvard Medical School, Produced in partnership with WGBH Educational Foundation". Harvard University. 2008. Retrieved 2009-03-11. "The 1968 categorization of the combined Sleep Stages 3–4 was reclassified in 2007 as Stage N3."). In animals, NREM can be divided into neocortical UP states, or periods of robust spiking activity ("ON"), and DOWN states, or periods where most neurons are silent or "OFF" (Steriade et al., 1993). A recent study by Miyawaki et al. (2017) found support for low activity NREM microstates in freely behaving rats ("LOW"), in addition to these UP and DOWN states, sometimes referred to as sleep small-amplitude irregular activity (S-SIA; Miyawaki et al., 2017; Pickenhain & Klingberg, 1967; Bergmann et al., 1987; Jarosiewicz et al., 2002). The SIA acronym was originally used to describe quiet waking patterns, so S-SIA will be referred to as LOW in this paper. Transitions between UP and DOWN states can synchronize global brain activity and provide a potential window for hippocampal-cortical information transfer (Rasch & Born, 2013; Sirota & Buzsáki, 2005). Additional activity patterns also characterise SWS including K-complexes (<1 Hz) arising from cortically generated slow oscillations and sleep spindles (7-16 Hz) and sharp wave ripples, containing a sharp wave

(0.5-50 Hz) and a ripple (100-300 Hz; Buzsáki, 2015; Cutsuridis & Graham, 2019), in the hippocampus.

Sleep spindles are generated by thalamocortical loops and observed in the primary sensory and prefrontal areas of the cortex (Lüthi, 2014). Sometimes called sigma waves, sleep spindles are bursts of activity with spindle-like appearances on EEG and are often accompanied by muscle twitches (Ulrich, 2016). Spindle density increases following learning in both humans and animal studies (Ulrich, 2016). A related phenomenon, K-complexes, often precede sleep spindles and are positively correlated with DOWN-UP state transitions and stored-trace reactivation (Johnson et al., 2010). Finally, sharp wave ripples are specific to the hippocampus and surrounding brain regions, and are associated with memory consolidation and reactivation, similar to K-complexes (Buzsáki, 1989).

REM sleep, sometimes called paradoxical sleep (PS), is characterised by a saw tooth theta rhythm (3-12 Hz) in the rat hippocampus and is accompanied by desynchronous cortical activity, similar to wake, and minimal muscular activity as detected by electromyography (EMG) with the notable exception of the eyes (Peever & Fuller, 2016). REM sleep is at the end of the sleep cycle and is associated with memory consolidation and learning (Hasselmo & Stern, 2014). Although the role of REM sleep in memory has been controversial due to the difficulty in isolating neural activity in REM sleep, direct involvement of REM sleep in spatial and contextual memory consolidation was confirmed in mice (Bandarabadi at al., 2019; Boyce et al., 2017) and the current theory proposes that both REM and non-REM sleep both contribute to memory consolidation in cognitively normal, healthy brains. Recent human fMRI studies show preliminary support for microstates within REM; specifically, phasic and tonic REM

(pREM and tREM, respectively; Wehrle et al., 2007). Phasic REM is characterised by limbic and parahippocampal activity and a lack of reactivity to sensory stimuli while auditory stimulation during tonic REM elicited activation of the auditory cortex. Thus, tREM is a period of residual alertness while pREM is a period of functional isolation within a closed intrinsic loop. Jing et al. (2016) found numerous potential substates in SWS and REM sleep using factor analysis. This suggests that tREM and pREM, in addition to other microstates, could be conserved between humans and non-human animals.

The precise frequency ranges described by EEG bands in both human and animal studies are somewhat arbitrary. Human EEG bands do not correspond exactly with their animal counterparts. A review by Corsi-Cabrera et al. (2001), observed that EEG bands used in animal studies were either arbitrarily determined, borrowed from human studies without consideration or no division at all was considered and that the lack of consensus among investigations was detrimental to the field. Another review (Corsi-Cabrera et al., 2000) noted that human studies had similar problems, with EEG bands rarely corresponding with EEG generators or with functional meaning of EEG rhythms.

To illustrate, the delta range is generally accepted as having a lower limit of 0.5 Hz, but researchers have used an upper limit of anywhere between 2 and 4 Hz. Sometimes even ranging from 6 to 12-14 Hz (Steriade & Deschenes, 1984). Such differences can arise from whether the animal is under anesthesia or not, due to the changes in the level of membrane hyperpolarization (Steriade & Llinás, 1988). This alone presents a challenge when discussing the properties of the delta range in various brain structures and the problem is only compounded with each subsequent frequency range.

Thus**, the second aim of this study is to examine the precise frequencies involved in EEG bands using non-arbitrary techniques such as time-resolved phase-amplitude coupling and determine the relevance of these frequencies with respect to states and substates/microstates within wake, NREM and REM, using the previously recorded EEG information gathered from the hippocampus and the primary motor cortex in Fischer-Brown Norway rats**.

1.3 Sleep and Motor Learning

Learning, or the acquisition stage of memory, can be separated into procedural learning and memory, largely non-hippocampus-dependent, and declarative learning and memory, hippocampus-dependent. This difference was most infamously demonstrated by the patient H.M. following a bilateral medial temporal lobectomy. With the loss of his hippocampus, H.M. lost the ability to form new explicit memories, though his procedural memory and working memory remained intact (Scoville & Millner, 1957, Eichenbaum, 2013).

The role of sleep in the storage, or consolidation, of declarative memory is well-established (Rasch & Born, 2013), but despite evidence for sleep improving performance of motor skills, a meta-analysis found no conclusive evidence that sleep enhances consolidation (Richard & Pan, 2017). Further investigation revealed a potential source of variance: baseline learning performance. In one study, offline gain in motor skill performance was dependent on the pre-sleep performance such that only performers of intermediate skill pre-sleep showed significant improvement post-sleep, with spindle counts correlated with the degree of improvement (Wilhelm et al., 2012). No such improvement was found in pre-sleep high or low performers. In another study,

performance only improved in fast learners and not slow ones (Albouy et al., 2008). A comparison of motor skill performance following daytime wakefulness or nighttime sleep showed better improvement following sleep (Rångtell et al., 2017). The same study also found that baseline performance levels played a role in improvement regardless of the whether wakefulness or sleep followed the learning period (i.e. high performers had smaller improvement than low performers regardless of whether they slept or not after learning). These improvements were only evident when the average retesting trials scores were divided by the last three learning trials and not the three best learning trials.

It is therefore reasonable to consider that some aspect of sleep contributes to the stabilization and enhancement of procedural memory. Thus, **the third aim of this study is to determine whether any changes to a state or due to a procedural memory paradigm** (i.e. mediated by non-hippocampal brain structures) **can be detected**.

Sleep phenomena may also exhibit differences induced by the procedural memory paradigm. Thus, **the fourth aim is to determine whether any extant phenomena affected by procedural learning, most especially during sleep, can be detected as well**.

1.4 Cross-Frequency Correlation

The electrical activity of neural networks observed as oscillations by EEG underlies cognitive functions such as perception, attention and memory (Canolty & Knight, 2010; Schroeder & Lakatos, 2009; Shirvalkar et al., 2010). They can form rhythms categorized by the frequency in Hz.

Additionally, different frequencies also have different spatial scales with lower frequencies modulating activity over larger spatial regions and higher frequencies

modulating activity over smaller spatial regions (von Stein & Sarnthein, 2000). Furthermore, neural network activity associated with stimulus processing differs depending on the phase of ongoing oscillations (Canolty & Knight, 2010). This gives rise to a class of complex temporal and spatial interactions between different rhythms known as cross-frequency coupling (CFC; Canolty & Knight, 2010). These rhythms have two key components that can be used to measure their interactions with other rhythms: amplitude and phase. The interactions can be phase-phase (PPC), phase-amplitude (PAC), or amplitude-amplitude (AAC) as shown in Figure 1.4.1. The most common analytical methods for PPC and AAC are susceptible to mathematical artifacts – a broad range of artificial and biological noise will produce results indistinguishable from coupled frequencies (Gerber et al., 2016). This leaves PAC as the most reliable method.

PAC is a type of CFC, also known as a nested oscillation, where the phase of one oscillation is coupled with the amplitude of another. Often, PAC describes the association between the phase of a lower frequency and the amplitude of a higher frequency (Canolty & Knight, 2010). It can be measured in a variety of ways including phase-locking value (PLV), mean vector length (MVL), Kullback-Leibler-based modulation index, among others. However, no preferred measure has yet emerged due to the relative limitations of each. Despite providing similar reliability and accuracy, the principle limitation was the inability to measure PAC strength (Samiee & Baillet, 2017; Tort et al., 2010). A methodological study by Samiee and Baillet (2017) refined existing PAC analytical techniques, allowing for greater temporal resolution, increased sensitivity and introduced a measurement of PAC strength. If tPAC provides a measures of PAC locally i.e. neuronal synchrony and integration within a region while inter-regional tPAC (IRtPAC)

assesses synchrony and integration between regions for PAC. With the issue of accurately detecting and measuring PAC resolved, the question remains: What rhythms are likely candidates with functional significance? While numerous rhythms can be coupled, interactions between theta and gamma oscillations are a hallmark feature of CFC in the hippocampus and have been implicated in a number of hippocampus-dependent functions (Lynn & Sponheim, 2016).

Selective optogenetic silencing of theta-rhythm generating cells during REM sleep impairs the formation of contextual memory while preserving other types of memory (Boyce et al., 2016). This impairment does not occur when these cells are silenced during non-REM (NREM) or wakefulness. Further investigation of this impairments reveals diminished theta-gamma oscillation PAC concurrent with impairment (Bandarabadi et al., 2017).

Cross-frequency coupling (CFC) within brain regions has been implicated in memory and memory-related functions. The strength of theta-gamma coupling in the hippocampus predicted performance accuracy in item-context learning tasks (item reward dependent on environmental context; Tort et al., 2009), matching-to-place tasks (six-arm radial water maze; Shirvalkar et al., 2010) and the T-junction working memory task (Yamamoto et al., 2014). The strength of theta-gamma coupling in cortical areas including the medial and lateral prefrontal cortex predicted performance accuracy during an attention task (Voloh et al., 2015). Working memory deficits across numerous modalities have been observed in people with schizophrenia (Lee & Park, 2005). During a variety of working memory tasks, those with schizophrenia had decreased theta and

gamma amplitudes, absent or abnormal gamma modulation and/or deficient synchrony when compared with controls (Lynn & Sponheim, 2016).

CFC has shown clinical relevance especially in disease states in both human patients and animal models. Declines in theta-gamma coupling preceded Aβ overproduction in a mouse model of Alzheimer's disease (Goutagny et al., 2013) and PAC during wakefulness and REM was diminished in APP-KO mice (Zhang et al., 2016). Cross-frequency coupling has been expressed by theta, gamma and other oscillations in numerous cortical areas in animal models including, the prelimbic cortex, cingulate cortex, retrosplenial cortex, the primary and secondary visual cortex, and the temporal cortex (Jing et al., 2016). Similar cortical involvement has also been documented in humans. In a study by Reinhart (2017), endogenous theta band coupling between the medial frontal cortex and the right lateral prefrontal cortex was non-invasively manipulated. In-phase stimulation in neurocognitively normal humans synchronized theta coupling and rapidly improved performance in a classical time-estimation task (Reinhart, 2017).

Reinhard (2017) also notes anti-phase stimulation impaired performance and desynchronized CFC, but that state could be immediately rescued by in-phase stimulation. The persistent neural activity and behavioural changes following stimulation suggests that this externally modified coupling changed the participants' behaviour as a result of neuroplastic changes in functional connectivity. These findings open up the possibility of drug-free interventions with bidirectional capability allowing for the impairment of excessive synchrony or the rescue of deficient synchrony (Reinhart, 2017).

While the presence of cross-frequency coupling within the waking brain has been firmly established, its presence within the sleeping brain is more nebulous. Memory, of any cognitive functions, seems especially sensitive to the strength of cross-frequency coupling, but whether that memory must be hippocampus-dependent has yet to be determined. There is a lack of data with respect to the simultaneous activity of both cortical and subcortical regions in regard to CFC and it is unclear whether a CFC interaction between brain regions plays a role in cognitive functions such as memory.

Due to this, **the fifth and final aim of this study is to determine whether the sensitivity of CFC to memory and learning is limited to hippocampus-dependent memory and the role of the cortex in the event of either outcome**.

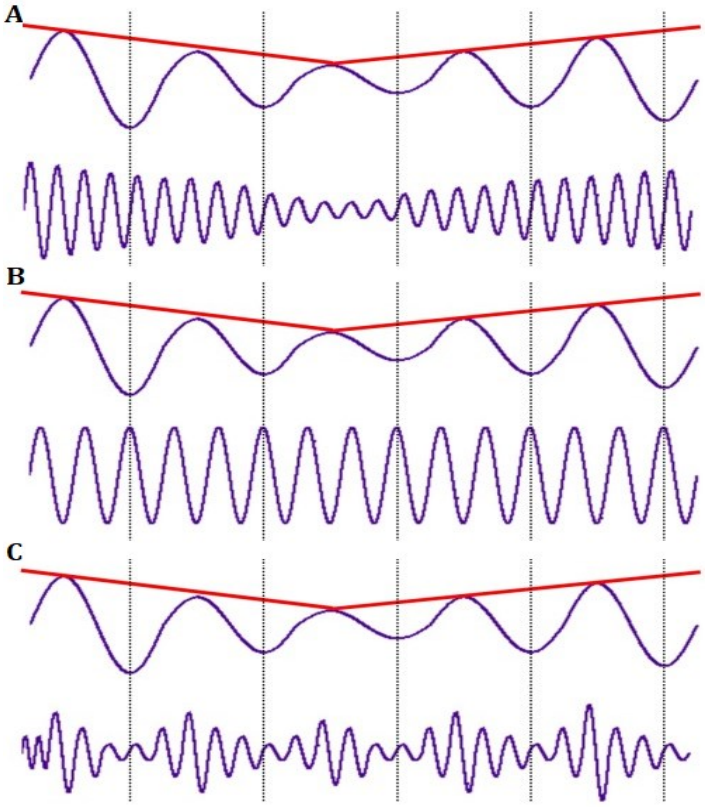

Figure 1.4.1: Types of Cross-Frequency Coupling. A) Amplitude-amplitude coupling. B) Phase-phase coupling C) Phase-amplitude coupling. Adapted from Jirsa and Müller, 2013, *Front Comput Neurosci, 7,* 78. Copyright 2013 Jirsa and Müller.

2. Materials and Methods

2.1 LFP Recordings

The EEG data used in this study was collected at the Tatsuno Lab of the Centre of Canadian Behavioural Neuroscience at the University of Lethbridge in 2015 and 2016. The data are from two groups of adult male Fischer-Brown Norway rats (two groups of n=3 for a total of n=6) with a sampling frequency of 2000 Hz. The data acquisition was part of a research program exploring transcranial direct and alternating current stimulation (tDCS and tACS, respectively). Twisted bipolar electrodes (~600 μm tip separation) were bilaterally implanted in the hippocampus and in the dominant hemisphere's primary motor cortex (this was the right hemisphere for all rats). Dominance was determined by observing the favoured forelimb used in the Wishaw reaching task paradigm during habituation. EMG electrodes were bilaterally implanted in the acromiotrapezius muscle. A single stainless steel ground screw was also implanted in each rat's cranium. The University of Lethbridge Animal Care Services and the Canadian Council on Animal Care guidelines were followed for all surgical and behavioral procedures. Two animals were excluded from the task analysis due to insufficient recording days shared with the other subjects as well as one animal that removed its recording electrode. Thus, the task data for only three animals was used. The stim conditions applied to each animal is listed in Table 2.1.1. These subjects shared four of twelve task days (Days 1, 3, 8 and 8) which were then analyzed. Figure 2.1.1 shows representative raw LFP recordings.

Table 2.1.1: Subject Stimulation by Task Day. Three subjects underwent the procedural learning task with the same timing. tDCS was delivered during pre-task REM. tACS was delivered during post-task SWS.

Rat \ Day	1	3	6	8
3	tDCS	tDCS	tDCS	tDCS
4	Sham	Sham	Sham	Sham
6	tACS	tACS	tACS	tACS

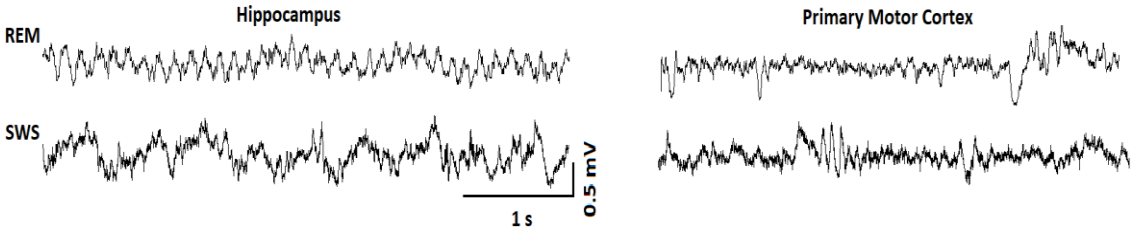

Figure 2.1.1 Raw LFP Data. For baseline, animals were placed in the sleep pot for approximately 2 hours uninterrupted. For task, animals had about 1 hour in the sleep pot followed by the reaching task in the reaching box. This was followed by another hour in the sleep pot.

2.2 Sleep Scoring

For automated sleep scoring, each recording was initially divided into motionless and non-motionless epochs according a movement threshold of 1.5 times the median of the EMG signal. The median was chosen for its resistance to outliers. Motion epochs less than one second were removed along with motionless epochs less than 20 seconds. The recordings were then down-sampled and band-pass filtered as an initial preprocessing step. In order to reduce fragmentation, SWS and REM epochs were merged within 5 seconds of each other and epochs with durations under 10 seconds were removed. Theta (5-12 Hz) and delta (1-4 Hz) were obtained from hippocampal CA1 recordings and applied to REM detected. REM epochs were found by calculating when a ratio of theta to delta power divided by EMG amplitude exceeded a threshold of the 85th percentile of the overall ratio during a motionless epoch. As the REM and SWS detection algorithms run

independently of each other, automated and manual checks were run to ensure no overlap. When an overlap occurred, epochs were either truncated or removed, depending on which ratio was larger. In addition, suspect REM epochs, periods that were scored as REM, but did not contain recognizable theta oscillations, that the automatic scoring script failed to remove were manually removed. SWS epochs were calculated by taking the ratio of delta power to theta power divided by the EMG amplitude. The SWS epoch threshold was also the 85^{th} percentile of the overall ratio. Motionless periods that failed to meet both the SWS and REM thresholds remained classified as wakefulness periods. These periods were not distinguished from wakefulness with motion over the threshold.

For manual scoring, baseline recordings with an available video were verified manually. Each 0.5 second was categorized as either "motion" or "motionless" and then checked against the automatic sleep score after a binary conversion (motion = 1, motionless = 0). Periods of motionlessness or non-motionlessness were required to have a minimum duration of 5 seconds. The automatic scores needed to agree within a 10% tolerance limit of the manual scores to be considered identical. Trials that failed the tolerance test were redone with increased thresholds until the trial passed the tolerance test. The hippocampal EEG traces of REM and SWS epochs were manually reviewed for characteristic theta sawtooth waves or large amplitude, slow wave oscillations (~1 Hz), respectively.

2.3 Behaviour Scoring

Security videos were available from a select number of baseline days for four of the six animals. Each 0.5 second segment was classified as one of five behavioural categories: motionless (M), sniffing/whisking (SF), grooming (G), head shift/movement (HS), and

body shift/movement (BM). Due to technical difficulties switching between the security camera and the high-speed reaching task camera, there were no videos of task days available for comparison.

2.4 tDCS and tACS Stimulation

Following baseline sleep recordings, task recordings were obtained for three of the six animals. These consisted of 1 hour of pre-task sleep followed by a ~30 minute Whishaw reaching task with a 1 hour post-task sleep session (Whishaw et al., 1986). The tDCS stimulation was delivered during pre-task REM and the tACS stimulation was delivered during post-task SWS (Figure 2.4.1). The task session length was dependent on the length of time it took for the animal to complete ten reaches. Animals in the stim condition received either 10.1 μA of DC stimulation or 10.1 μA, 0.8 Hz of AC stimulation with the electrode in the motor cortex and the cathode in the deep posterior brain. The duration of the stimulation was 30 seconds with a cumulative maximum of 600 seconds or 20 stimulation episodes. Stimulation was administered with a delayed onset of 10 seconds. Acquisition runs where stimulation was not delivered were listed as sham trials. Stim time points were tracked and eliminated from the analyzed recording data.

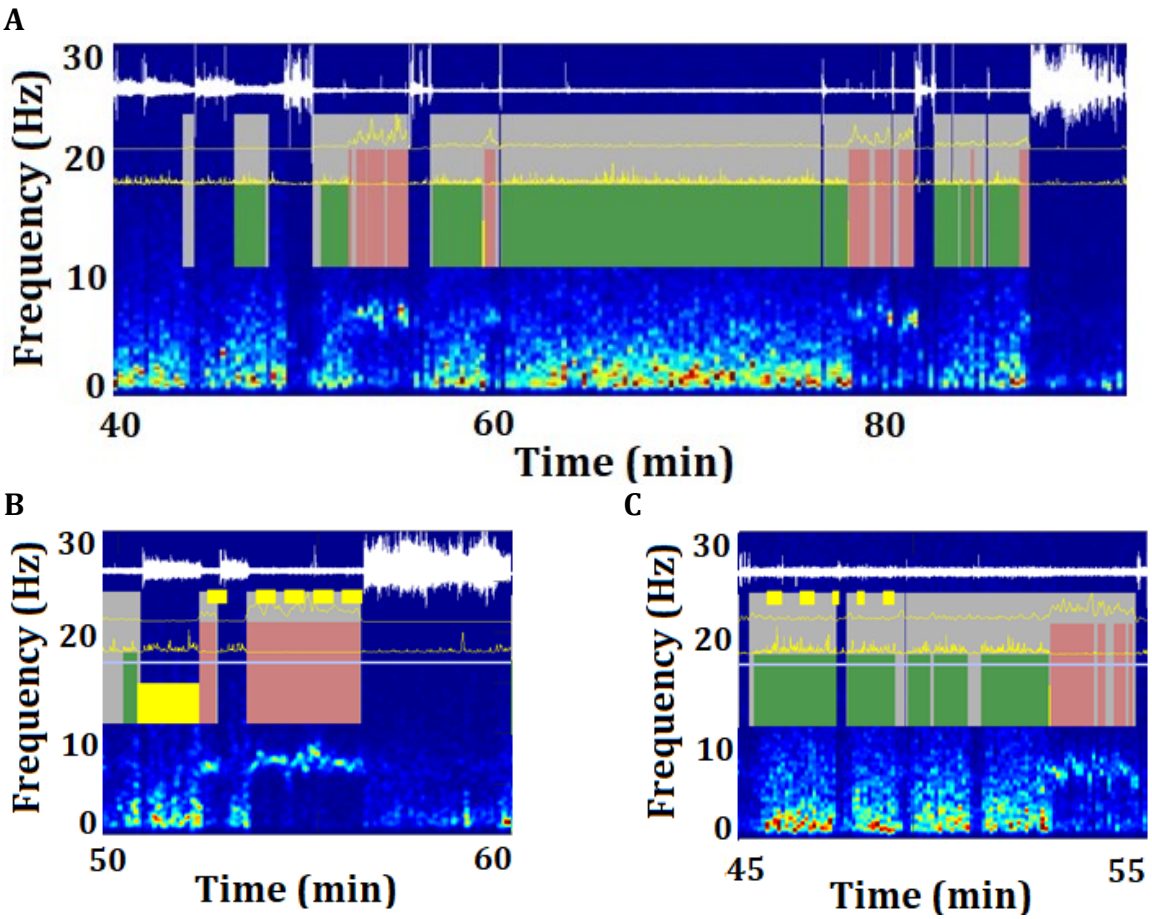

Figure 2.4.1: Representative Sleep Scored Spectra and Traces. EMG (white overlay) used to detect motionless periods (grey). Ratio of spectral power between delta and theta bands (REM: upper yellow trace, SWS: lower yellow trace) used to calculate SWS (green) and REM (red) periods. A) Baseline/Sham sleep score without stimulation in either REM sleep or SWS. B) Pre-task REM sleep tDCS of 10 µA (upper yellow overlays). SWS and REM epochs that extended into non-motionless periods were truncated (lower yellow overlay). C) Post-task SWS tACS of 10 µA at 0.8 Hz.

2.5 Dimensionality Reduction

Following the initial pre-processing and sleep scoring step, the power spectrum was estimated for each brain state using the multi-taper time-frequency spectrum – continuous process function from Chronux (Mitra, P. & Bokil, H., 2008). Chronux is documented and freely available for download from http://chronux.org/. The spectrogram was then log-transformed and analysed using the Matlab principal component analysis (PCA) function. PCA is a statistical procedure that uses an orthogonal transformation to

convert data containing possibly correlated variables into a values of linearly uncorrelated principal components. The transformation calculates maximal variance, so that the first principal component and eigenvector have the largest possible variance. The second principal component has the second most and so on. Following the PCA transformation, the data was projected onto the top three eigenvectors. The top components were selected according to three criteria, which is shown in Figure 2.5.1. First, the total explained variance was at least 90%. Second, the last component's eigenvalue was at least double that of the following component's value. Third, the eigenvalues included were above the "elbow" on a scree plot where the slope of the eigenvalues changes. Although these can be considered subjective measures, no method has been proven to be any better or worse than any other and remain acceptable methods of selecting components.

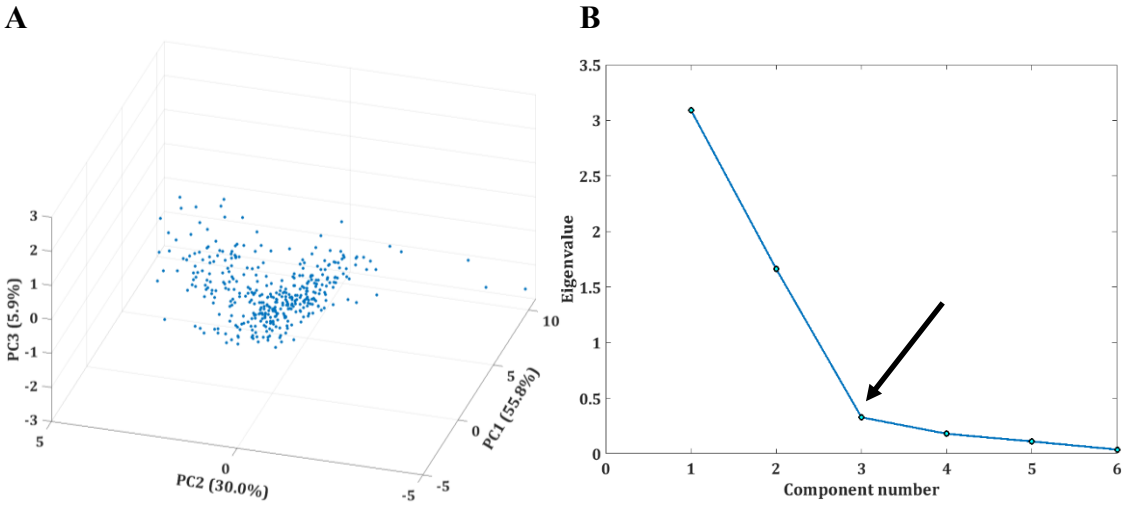

Figure 2.5.1: Principal Component Selection. A) Principal component plot with the total variance explained of each. Components were chosen to have a cumulative variance explained of at least 90%. B) Scree plot with elbow indicated by arrow. Components above elbow were kept and those below were disregarded.

2.6 Coherence and Cross Power Spectral Density

Correlation (*r*) and coherence (*coh*) are very similar; correlation is a means of determining the extent to which two variables covary over time and can be expressed as a

normalized score between -1 and 1 while coherence determines the similarity of two variables covary across frequencies. Autocorrelation or self-coherence can describe how well a signal is correlated to itself across multiple time points, but in the case of multiple signals, especially without temporal cues of some kind, the differences between correlation and coherence can become large. In the signals recorded by LFP, coherence is the more appropriate method although there is a high comparability between the two (Guevara & Corsi-Cabrera, 1996; Eberly, 2016). Figure 2.6.1 illustrates the differences between coherence and correlation. Although correlation and coherence are similar, there can be signals that are coherent and not correlated. Coherence, or magnitude-squared coherence, is a function of frequency with values between 0 and 1 indicating the degree of coherence i.e. how well the amplitude of one signal corresponds to another at each frequency. It is a function of the auto power spectral densities, $P_{xx}(f)$ and $P_{yy}(f)$, given by the equation:

(3)

$$C_{xy}(f) = \frac{\left|P_{xy}(f)\right|^2}{P_{xx}(f)P_{yy}(f)}$$

The significance level for coherence is given by coherency as described in the following equation defined by Shumway and Stoffer (2017), pg. 212, equ. 4.105:

(4)

$$C_{\alpha} = \frac{F_{2,2L-2}(\alpha)}{L - 1 + F_{2,2L-2}(\alpha)}$$

where F is the inverse of the cumulative distribution of the F-distribution, α is the probability of a type I error, and L is the number of degrees of freedom, approximately n*B, where n is the number of observations and B is the bandwidth. The Matlab script for

this equation was adapted from the original script created by David M. Kaplan (2004), which is freely available for download. There is another reason correlation is not an ideal measure for LFP recordings: volume conduction. Field potentials in the brain are an epiphenomenon of electrical activity in both single cells and cell ensembles, and thus, the signal may have almost any relationship with the contributing source or sources. Field potentials are present even in regions where the units are not firing when there are subthreshold afferent activity or inhibitory currents. Localizing the signal is of critical importance regardless of scale due to Ohm's Law (V = IR), which describes the proportionality between voltage (V) across a conductor of resistance (R) in an electrical circuit and the current (I) flowing through the system. The consequences of this principle are well-known: despite efforts to record from purely proximal sources, LFP has become infamous for distal sources and sinks contributing to the "local" potentials. These sources and sinks, by virtue of the transmission of the charge through space (i.e. current), may be considered as generators of the recorded potential.

To identify and measure the contribution of current generators to the LFP signal, current source density (CSD) methods have been widely implemented. The cross-spectrum of two signals x(t) and y(t) is defined as the Fourier transform of the covariance function of x and y. The cross power spectral density (CPSD) $P_{xy}(\omega)$ is determined from the ensemble average of the Fourier transform of x(t) multiplied by the complex conjugate of the Fourier transform of y(t). Thus, the CPSD is said to be the Fourier transform of the cross-correlation function. The cross power spectral density is the distribution of power per Hz and is defined as:

(5)

$$P_{xy}(\omega) = \sum_{m=-\infty}^{\infty} R_{xy}\,(m)e^{-j\omega m}$$

where $R_{xy}(m)$ is the cross-correlations sequence. As such,

signals with zero phase lag, while having high correlation and potentially high coherence, would likely be volume-conducted. While in human scalp EEG, correlation is often used as there are other methods for accounting for volume conduction, in this study, only coherence and CPSD will be considered. The methods of correcting for volume conduction in scalp EEG studies are often computationally complex and involve calculations between multiple paired electrodes which were not available for this study.

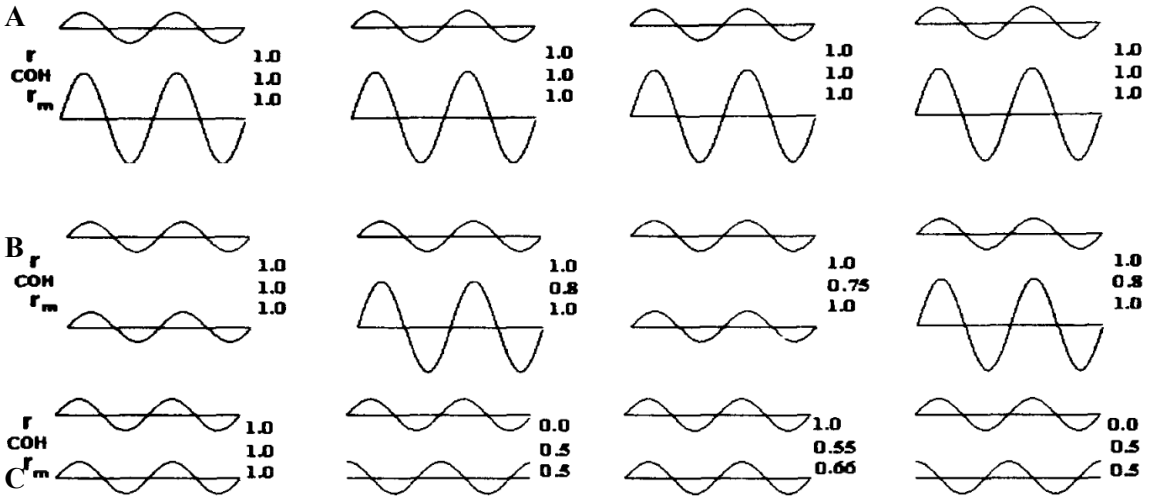

Figure 2.6.1: Coherence and Correlation. The Pearson product-moment coefficients at 0 lag (*r*) and coherence (COH) values for each 1-s epoch, and the mean *r* (rm) and *coh* for the successive four epochs are given for each pair of signals. Voltage and phase were manipulated in one of the signals of each pair. Voltage was multiplied by 3 in A and B. Phase was delayed by 90 degrees in B and C. A illustrates that in signals with both a consistent amplitude and phase to each other, coherence and correlation produce the same result while in B and C, changes in either amplitude or phase can influence coherence and correlation to different extents. Adapted from Guevara and Corsi-Cabrera, 1996, *Int J Psychophysiol, 23,* 145-153. Copyright 1996 Guevara and Corsi-Cabrera.

2.7 Time-Resolved Phase-Amplitude Coupling

Following pre-processing and sleep scoring, CFC analysis was carried out. The cortical and hippocampal recordings were imported into the Brainstorm interface (Tadel

et al., 2011), which is documented and freely available for download online under the GNU general public license (http://neuroimage.usc.edu/brainstorm). The recordings were segmented into epochs of equal lengths and analyzed using tPAC and IRtPAC as introduced by Samiee and Baillet (2017) and then averaged. The equation for phase-amplitude coupling where the amplitude a fast frequency A_{f_A} with a frequency f_A is modulated by the phase, ϕ_{fp}, of a slower frequency, $f_P$and $f_P < f_A$ is as follows:

(6)

$$\begin{cases} \overline{z} = \dfrac{\int_0^{t_p} A_{f_A}(t).e^{\phi_{fp(t)}}\,dt}{\sqrt{\dfrac{1}{t_p}\int_0^{t_p} A_{f_A}^2(t)\,dt}}, tPAC = |z|, \qquad \phi_{tPAC} = angle\,(\overline{z}) \\ t_p = \dfrac{1}{f_p^*} \times \underset{k:integer>1}{\operatorname{argmax}} \{k \times 1/f_p^* \leq \Delta\} \end{cases}$$

Where

t_P: data length for averaging (equal or less than sliding window length)

k: n full cycles of f_P in the sliding window

$A_{f_A}(t)$: amplitude envelope of $x_{f_P}(t)$

$x_{f_P}(t)$: bandpass filtered signal of centre frequency of f_A

In this methodology, a range of potential frequencies of phase (f_P^*) can be entered with the caveat of a sliding window large enough to contain at least 1 cycle of the slowest frequency in the range. For example, if the sliding window is 1 second long, then the lowest end of the range of frequencies of phase must be at least 1 Hz. The test can be run sequentially, so if the frequency of interest is faster than the minimum in the first run, a second run be done with smaller windows and increased temporal resolution as a result. The coupling strength of (f_P, f_A) is given by a two-dimensional comodulogram.

2.8 K-Means Clustering

The PCA component score was passed as an argument into the k-means++ clustering algorithm. Rather than analyze the entirety of the random variables in the untransformed dataset, the three-dimensional projection of the dataset was clustered. The selection of the optimal *k* number of clusters for each CVI was generated by creating a matrix of k-means results using a range of clusters (k=1:15) and passing the results through one of three CVI evaluation functions: Calinski-Harabasz (CH), Davies-Bouldin (DB) and Silhouette (SH). CVI performance was determined from behavioural relevance (whether the resulting clusters were separated according to some metric of behaviour such as intensity and type) and whether there was significant distinction between the variable and clusters statistics of each mean cluster. Clustering was carried out on individual sessions before being aggregated through tolerance testing.

Mean cluster spectra were derived for each sleep state under each condition through selection of initial prototype clusters (Pascual-Marqui et al., 1995) followed by double-layered tolerance testing where successive clusters were compared to each of the prototypes and determined to be similar and concatenated together or dissimilar and the cluster listed as a new prototype. Clusters within a relative tolerance of 5% were concatenated with the given prototype provided delta and theta ranges were also within 95% similarity. Clusters outside the tolerance limits were set as new prototypes. Delta and theta ranges were selected as key tolerance limits due to the high coherence previously found in those ranges. For the sake of simplicity, only microstates detected in multiple sessions were considered. Once all the clusters were assigned to a prototype, variable and cluster statistics were extracted and the prototypes evaluated as microstates.

Variable statistics included band power and the peak amplitude and its associated frequency for each band. Five bands were selected: delta, theta, spindle, gamma and ripple. Cluster statistics included two metrics: 1) lifespan, or duration of a cluster, and 2) cluster coverage, or the ratio of the total time assigned to a given cluster over the total recording time. These metrics give a measure of the stability of a given cluster class. Duration was determined by labelling the spectra bins with their respective timecode and then determining which bins were adjacent following clustering. The average number of adjacent bins was than multiplied by the bin length to create an average duration. For each spectra, the incidence rate of adjacent groups of bins was also counted to control for spectra that consisted of noise (no adjacent bins) or single occurrences (all bins in cluster are adjacent).

2.9 Statistical Analysis

CFC data analysis was performed with Brainstorm. Additional analysis was carried out using Matlab 2018a and SPSS 24. Pair-wise comparisons are reported using an F statistic. Bonferroni corrected p-values were used to determine significance for all multiple comparisons tests.

3. Results

Three key goals underlie this project: 1) the establishment of microstates through arbitrary, semi-arbitrary and non-arbitrary means, 2) the effectiveness of semi-arbitrary and non-arbitrary techniques in detection of brain states and microstates, and 3) the effect of procedural learning on microstates. The relationship between these goals and the five hypotheses of this project is shown in Figure 3.0.1. EEG synchronicity, which underlies communication between regions and facilitates coherent cognition and behaviour (Varela et al., 2001; Ward, 2003) was examined using coherence and CPSD as semi-arbitrary metrics under naïve and learning conditions, as well as in the presence of two stim conditions: tDCS and tACS. Second, CFC both within and between regions was examined using tPAC and IRtPAC, respectively, as arbitrary metrics. Third, k-means clustering analysis was carried out on dimensionally-reduced data projections and evaluated for potential microstates. Fourth, clustering was compared against behaviour in naïve animals to determine correspondence between clustering and behaviour. Finally, clustering was carried out on motion scored datasets to assess the ability of PCA and k-means clustering as non-arbitrary techniques to distinguish between brain states.

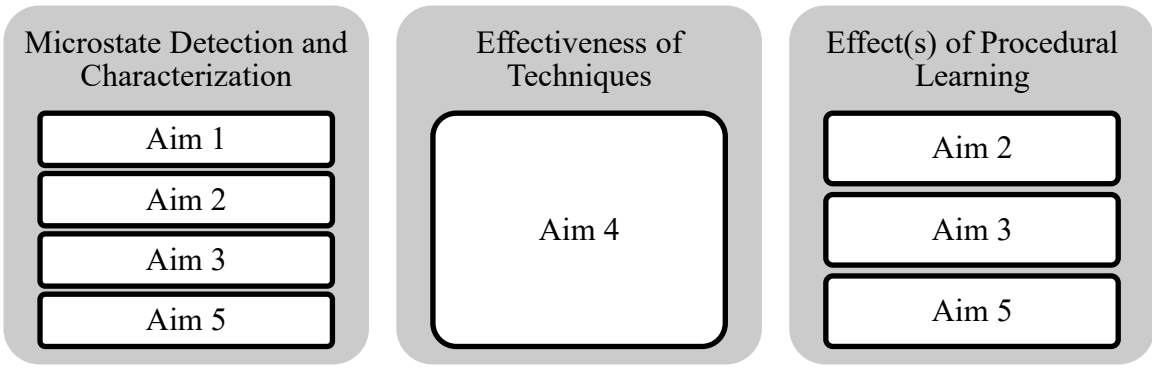

Figure 3.0.1: Grouped Aims.

3.1 Clustering of Sleep-Scored Data Reveals Stable and Transient Microstates

To investigate the presence of microstates, mean cluster spectra were generated

from the normalized spectra of the k-means clustering data points. To detect the presence of microstates, two sets of cluster features were first extracted: 1) variable statistics, or the characteristics of the data within a cluster, and 2) cluster statistics, or the characteristics of the cluster itself. In this study, cluster lifespan and coverage were used as cluster statistics (See Section 2.8). Tolerance tests were carried out to establish mean clusters such that clusters with features within tolerance of each other were merged together while those with features outside of the tolerance tests were kept separate.

The tolerance tests resulted in three SWS microstates: ON, OFF and LOW (See Section 1.1). Four REM microstates were differentiated as well: two consistent with tREM and pREM and two that greatly resembled cortical SWS spectra. Figure 3.1.1 shows representative SWS and REM microstates from pre-task sham to illustrate. Note that the bins are not a continuous time series, but discrete units. There is some overlap between ON and OFF states, but not sufficient to exceed tolerance.

REM and SWS classes were compared using a two-layer tolerance test. If 95% of the spectrum of interest was within 95% of the values of the contrasting spectrum, they were considered spectrally identical. While the hippocampal REM and SWS states were distinct, there was overlap between the cortical states. Figure 3.1.2 shows cortical SWS-like REM spectra and their SWS counterparts that failed the tolerance test i.e. were within 95% tolerance of each other. Figure 3.1.3 shows the power spectral density plots of these microstates. There were two transient cortical clusters spectrally similar to a SWS counterpart; these can be categorized as a high amplitude delta range cluster and a neocortical high gamma cluster. These clusters were present in baseline, all pre-task

conditions and post-task tDCS. There was no significant difference in the variable or cluster statistics between any of the conditions (p=0.87).

Table 3.1.1 shows the two cluster statistics of the REM and SWS microstates. Consistent with the literature, the LOW microstate had an extended lifespan well above either the OFF or ON states. The corresponding cortical state also had an extended lifespan. Among the SWS-like REM microstates (SR1 and SR2), the state corresponding with the neocortical ripple state (SR2) was less prevalent than the high delta state (SR1). Among the REM states in both the hippocampus and cortex, tREM (high amplitude theta; R2) was less prevalent than pREM (increased power across multiple bands; R1).

The states using PCA and k-means techniques support previous findings in the literature including the ON, OFF and LOW SWS states as well as the tonic and phasic REM states. Furthermore, SWS-like REM states were also detected and suggest local disconnect between the primary motor cortex and hippocampus-led global brain state.

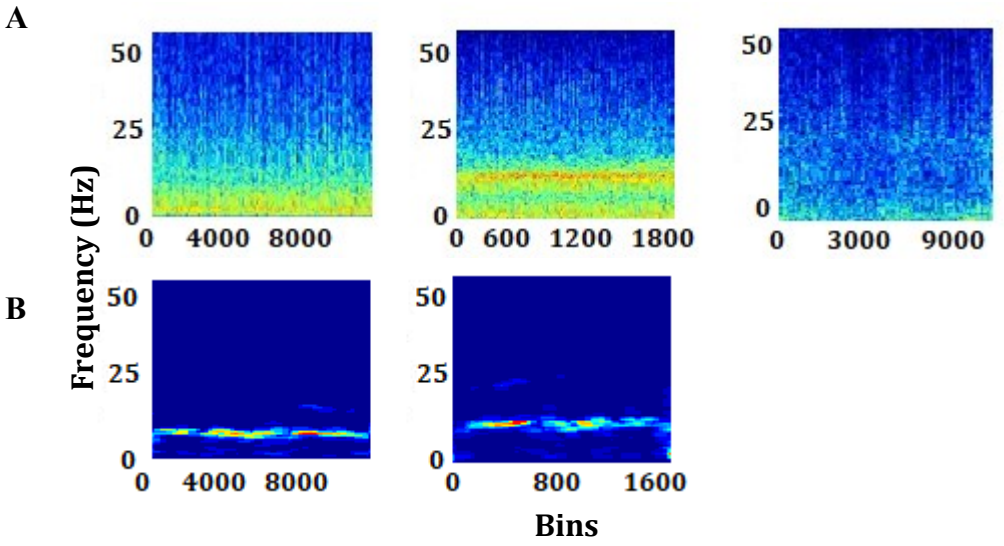

Figure 3.1.1: Mean Spectrograms for SWS and REM Clusters. A) Mean SWS clusters for pre-task sham (1 subject, 4 sessions). Left to right: DOWN, UP, LOW. B) Mean REM clusters for pre-task sham. Left: tonic REM (~6 Hz), Right: phasic REM (~8 Hz)

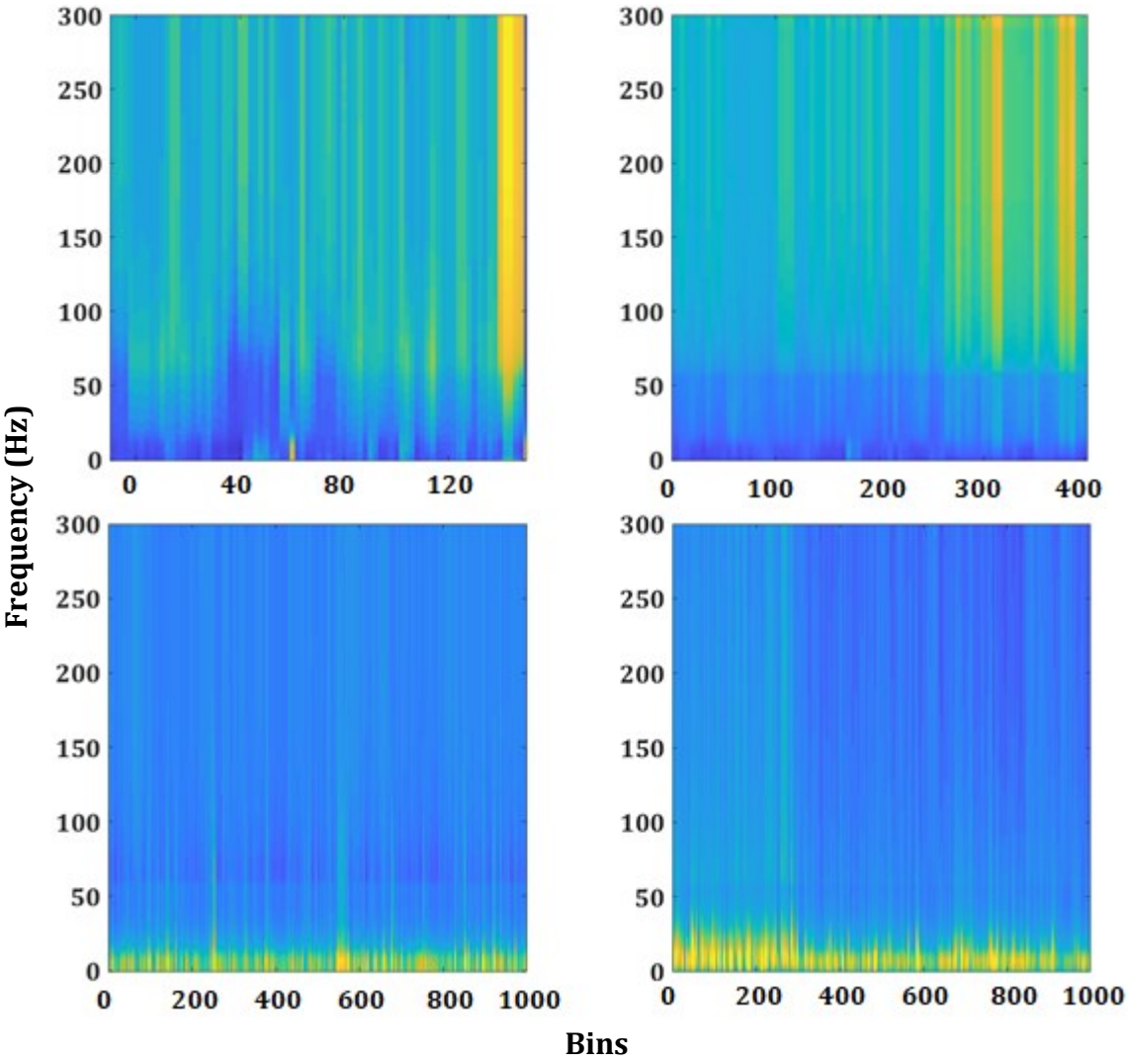

Figure 3.1.2: SWS-like REM Cluster Spectrograms in the Primary Motor Cortex. Left: REM, Right: SWS. 1 subject, 4 sessions.

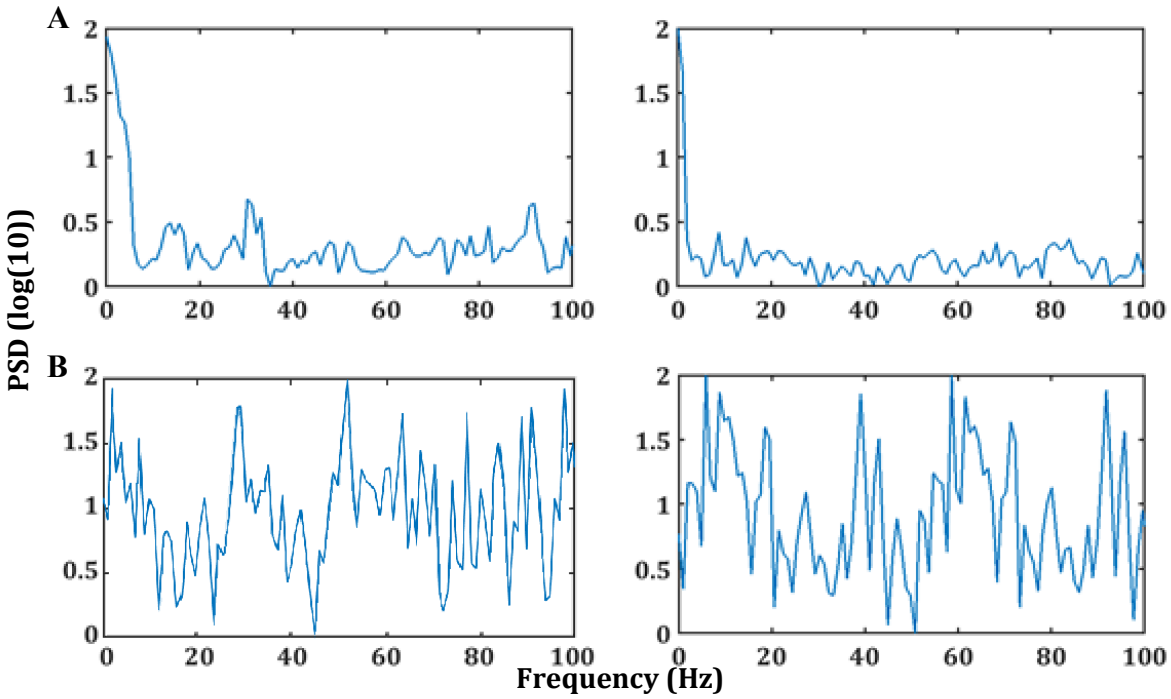

Figure 3.1.3: SWS-like REM Microstate Power Density. A) High amplitude delta state B) Neocortical ripple state. Left: REM, Right: SWS. 1 subject, 4 sessions.

Table 3.1.1: Features of Cortical and Hippocampal Microstates. S: SWS, R: REM, SR: SWS-like REM. Values are presented as mean ± SEM. 43 total sessions from 3 subjects.

Cluster Statistics							
Cortex							
Features	S1	S2	S3	R1	R2	SR1	SR2
Coverage (%)	39.49	19.40	41.76	42.84	8.82	40.39	5.35
SEM	0.00	0.02	0.00	0.06	0.00	0.00	0.00
Lifespan (sec)	1.73	2.19	8.09	2.59	1.39	2.12	1.17
SEM	0.12	0.06	0.14	0.02	0.00	0.02	0.00

Hippocampus					
Features	S1 (ON)	S2 (OFF)	S3 (LOW)	R1	R2
Coverage (%)	33.65	29.00	7.25	65.74	34.75
SEM	0.00	0.00	0.02	0.00	0.04
Lifespan (sec)	1.08	1.25	5.41	4.02	2.30
SEM	0.93	0.05	0.07	0.58	0.08

3.2 K-Means Clustering Sensitive and Specific to Behaviour

To investigate whether clustering had behavioural relevance, cluster sequences were compared against baseline behaviour scoring. Three aspects of the distribution of

behaviour between different clusters were focused on: 1) the separation of motionlessness from non-motionlessness i.e. sniffing, grooming, etc., 2) the degree to which a given cluster only contained a single behaviour, and 3) the degree to which a behaviour was contained in a single cluster. Given the variability of the maximum number of clusters and the triangular separation of the three most extreme behaviours (motionless, minimal movement and maximal movement), the three clusters at the vertices of the triangular separation were used to analyze behavioural distribution. The primary behaviour of the cluster at each vertex was used to classify them such that the top vertex was classified as the motionless cluster (M), the left vertex was classified as the minimal movement cluster (SF) and the right vertex was classified as the maximal movement cluster (BM). Only the Calinski-Harabasz-evaluated clustering results are shown due to its significantly more frequent detection of the motionless cluster across sleep stages compared with Davies-Bouldin and Silhouette (Bonferroni: $p < 0.001$; See Figure S8 for examples of Davies-Bouldin and Silhouette)

Figure 3.2.1 shows a representative k-means clustering plot. The cortical plot for the sleep scored data illustrates the triangular distribution of three key clusters: 1) a motionless cluster at the peak positive y-axis position, 2) a minimal movement cluster at the peak negative x-axis position, and 3) a maximal movement cluster at the peak positive x-axis position. The hippocampus rarely distinguished the motionless cluster and is not clearly distinguishable in either the sleep scored (top right) or motion scored (bottom right) data sets.

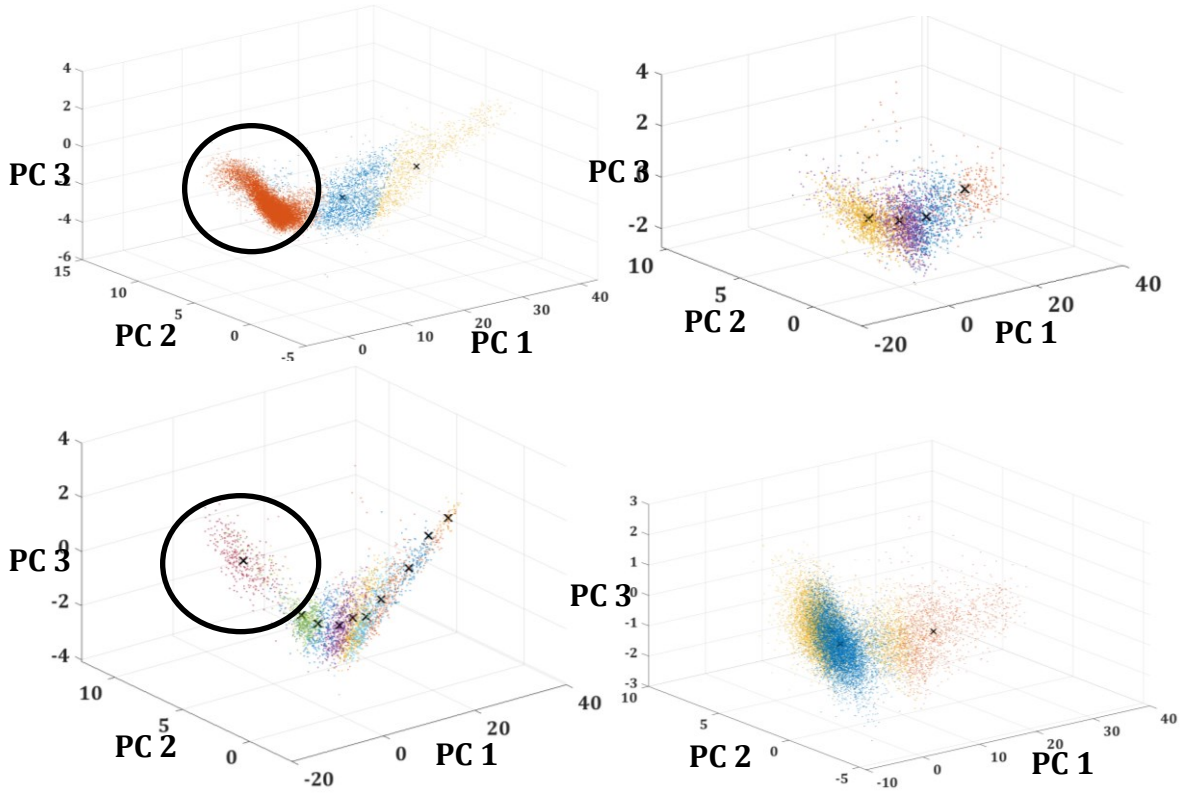

Figure 3.2.1: Representative Clustering in Sleep Scored and Motion Scored Data. Top: Motion Scored, Bottom: Sleep Scored. Left: Cortex, Right: Hippocampus. Black circle: Motionless cluster. The x-axis is the first principal component and the y-axis is the second principal component.

Figure 3.2.2 shows the mean cluster counts in baseline and task (No statistical difference was found following paired t-tests with cluster strength accounted for; p-value 0.92; see figure S10). There was a significant difference between the cortical and hippocampal clusters counts for wake and REM in baseline and pre-task sham. Baseline SWS was also significantly different while pre-sham SWS approached significance (p=0.07). In contrast, there was a significant difference in post-task sham for SWS, which was shared by post-task tACS. All other conditions showed no difference between cortex and hippocampus. Thus, naïve and pre-task sham exhibit increased local clustering in the primary motor cortex during wake and REM while post-task sham and tACS have increased cortical clustering during SWS.

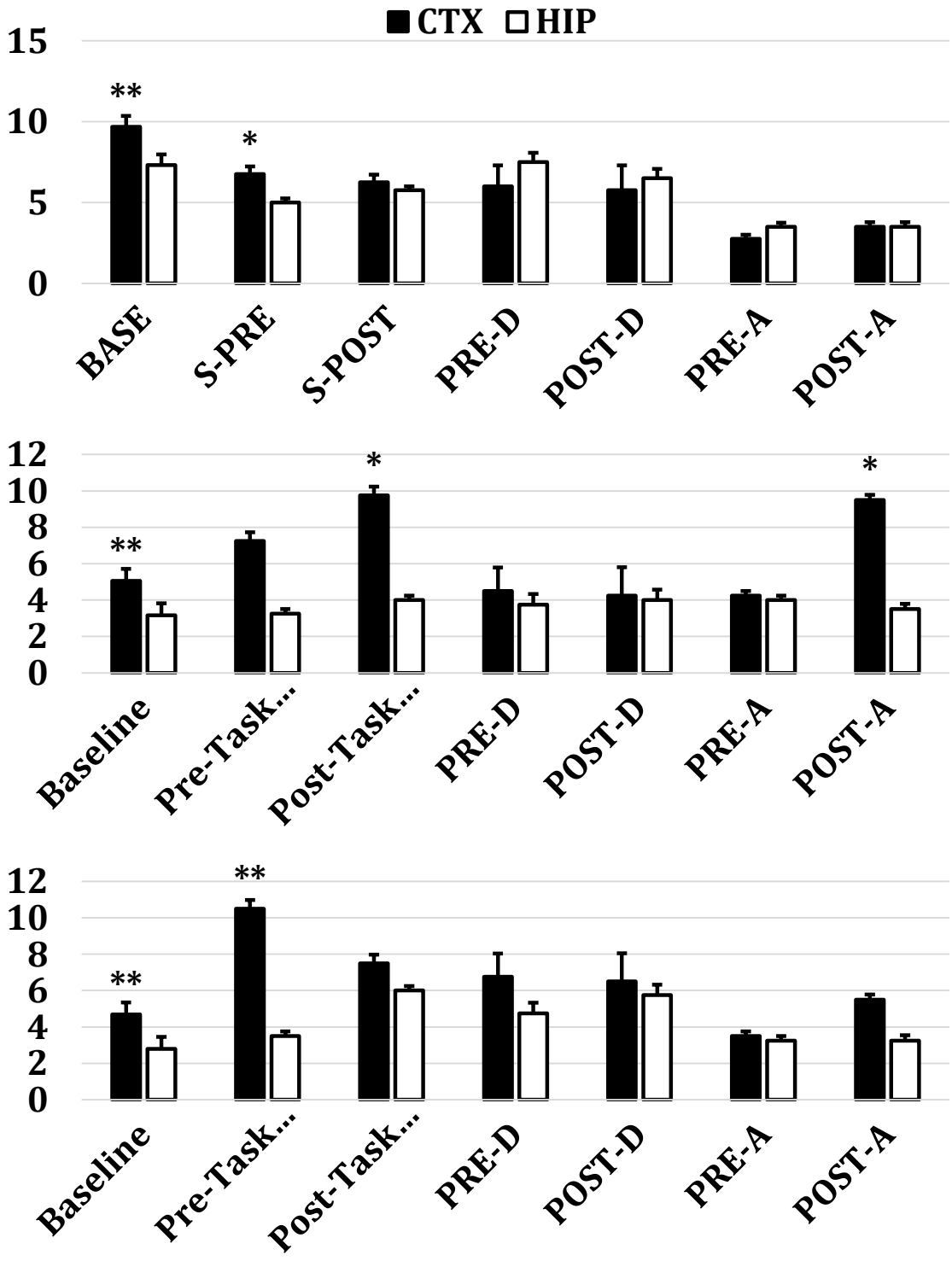

Figure 3.2.2: Cluster Count Comparison in Baseline and Task. Baseline cortical counts were significantly higher than hippocampal counts in all three brain states. * $p < 0.05$ ** $p < 0.01$. Top: Wake, Middle: SWS, Bottom: REM. BASE: Baseline, S-Pre: Sham Pre-Task, S-Post: Sham Post-Task, Pre-D: Pre-Task tDCS, Post-D: Post-Task tDCS, Pre-A: Pre-Task tACS, Post-A: Post-Task tACS

Figure 3.2.3 shows the inverse relationship between maximal movement and minimal movement and illustrates the tendency of the algorithm to overfit. Clusters along the horizontal axis contained a mixture of minimal, moderate and maximal movements. From left to right, the percentage of the cluster that was classified as minimal movement decreased while maximal movement increased. Four clusters can be visually distinguished, but the central "mixed behaviour" cluster had a tendency to be overfit.

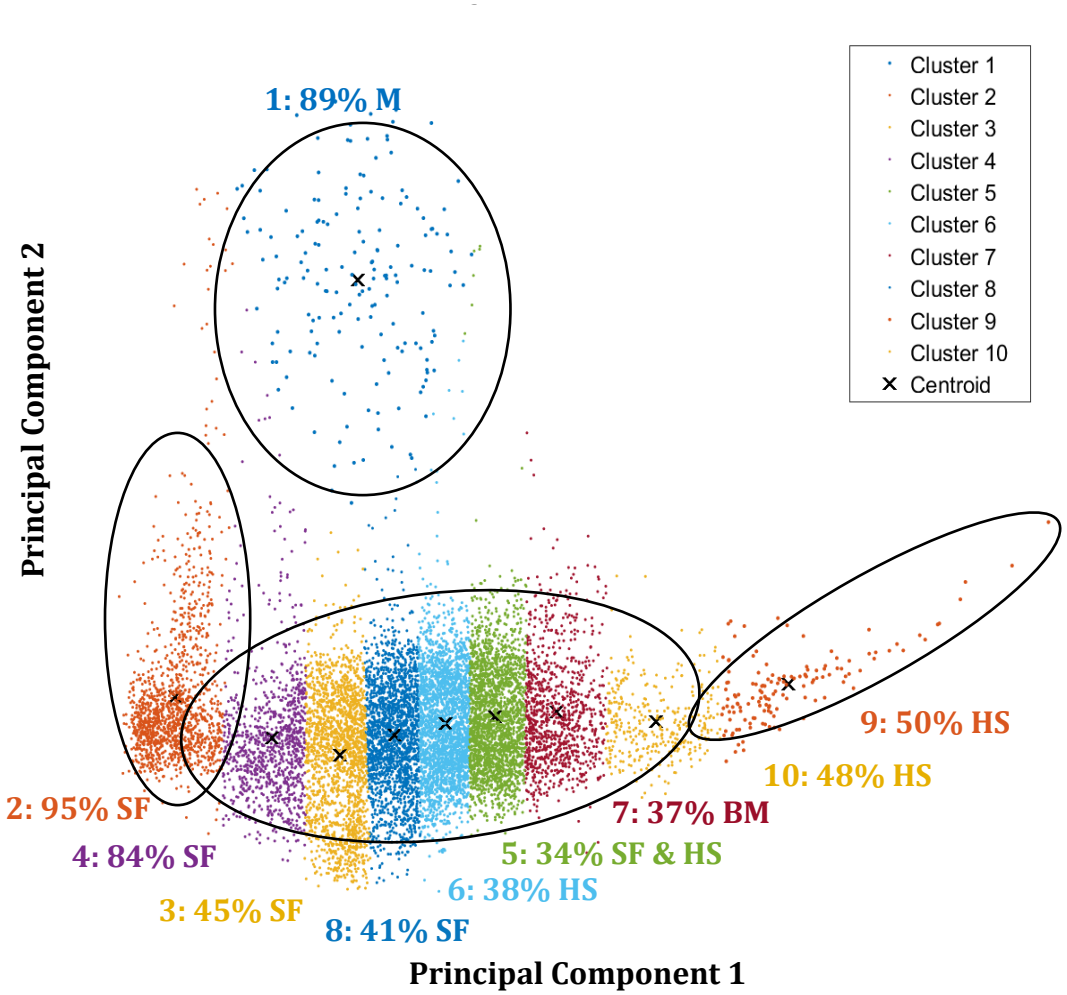

Figure 3.2.3: Inverse Horizontal Relationship of Minimal and Maximal Behaviour. Values indicate the cluster and then the percentage of the cluster described by the predominant behaviour within it. Black circles indicate intuitive clusters. The central cluster, containing compound behaviours, suffers from overfit. The purest behaviours at the three apices are more clearly separated than the central compound behaviours, which create a spectrum of behaviour differentiated by the clustering algorithm.

The wake motionless cluster was only distinguished in the cortex by CH evaluation (91.7% of clusters). Davies-Bouldin (15.3%) and Silhouette (0%) did not sufficiently distinguish the motionless cluster to be used in behavioural analysis. The cortical clustering separated the motionless cluster from the non-motionless ones significantly more frequently than in hippocampal clustering ($p < 0.001$). It should be noted that only two of the three subjects had videos (11 baseline days) for behavioural analysis.

Table 3.2.1 shows the cluster specificity (the percentage of the cluster that is a given behaviour) by primary behaviours and sleep stage. Cortical clusters were significantly more specific than hippocampal ones with respect to Wake motionless (Tukey's Student-t test; $p<0.05$) and REM maximal movement clusters (Tukey's Student-t test; $p<0.05$). Maximal movement during all three brain states was significantly less specific than those of either minimal movement or motionlessness (Tukey's Student-t test; $p<0.01$). Body movement during different sleep and wake states was not clearly differentiated between them and merged into a single cluster. In contrast, minimal movement and motionlessness were highly specific to the sleep stage.

Table 3.2.1: Behavioural Specificity in Sleep Scored Clusters. Clusters were selected using Calinski-Harabasz evaluated for this analysis. n = 11 (2 subjects).

		Wake			SWS			REM		
Region	Value	M	SF	BM	M	SF	BM	M	SF	BM
CTX	Mean	89.4	88.1	56.4	91.4	92.0	28.4	99.2	93.5	41.3
	SEM	4.2	3.8	5.5	3.6	3.2	6.7	0.8	2.5	9.4
HIP	Mean	58.9	74.3	50.2	76.9	90.1	15.4	97.1	90.8	18.3
	SEM	6.8	4.3	5.1	22.5	2.5	4.9	3.4	2.9	6.4

Table 3.2.2 shows the behavioural sensitivity (the percentage of a behaviour found in a given cluster) of clusters derived from sleep-scored data. Although motionless and minimal movement clusters were highly specific to brain states, they were noticeably

less sensitive. The cortex clustering was more sensitive to wake minimal movement ($p<0.05$).

The wake motionless clustering and REM maximal movement clustering were both sensitive and specific. REM maximal movement clusters were unexpectedly the most sensitive and the least specific. Clustering of behaviour, while specific to primary behaviours at the vertices of distribution, was less sensitive. This is consistent with only the vertices containing the extremes of the behavioural distribution while other clusters on the axis contained mixtures of complex behaviours such as grooming, exploratory sniffing, head movement, etc. The occurrence of pure behaviour (pure motionlessness, pure whisking, etc.) would be considerably less than the occurrence of mixtures of the these and other behaviours.

Table 3.2.2: Behavioural Sensitivity in Sleep Scored Clusters. n = 11 (2 subjects).

		Wake			SWS			REM		
Region	Value	M	SF	BM	M	SF	BM	M	SF	BM
CTX	Mean	79.8	26.8	13.5	35.8	39.8	41.9	44.7	36.8	61.6
	SEM	5.4	5.8	3.1	9.2	7.5	8.7	6.2	3.6	9.8
HIP	Mean	57.3	12.8	5.5	23.6	33.0	47.0	25.3	56.1	63.5
	SEM	19.5	3.1	1.2	9.5	3.3	5.9	6.0	5.4	5.0

The behavioural distribution of the motion scored clusters was then investigated to further establish the suitability of the selected algorithm and evaluation indices. The motion scored clusters were the same recordings as the scored ones, but without sleep scoring. The clusters were characterized as “Wake,” “SWS” or “REM” according to the predominant epoch contained within them. Behaviour was tracked according to the originating sleep stage such that under a behavioural category, there would be up to three subcategories indicating the sleep-scored epoch i.e. under head shift, there would be head shift – wake, head shift – SWS and head shift – REM. The gross behaviour was the total

of all behaviour regardless of origin while epoch behaviour was the percentage of the gross behaviour originating in a specific epoch. As such, the behaviour does not change, just whether it is all of the behaviour or the behaviour from a specific period of time. For each of the clusters, the corresponding epoch was used for this relationship such that for the motionless wake cluster, the epoch total would be the percentage of the gross behaviour that originated in wake clusters.

Table 3.2.3 shows specificity of the motion scored clusters for the gross and epoched behaviour. While the clusters were less specific to the total behaviour, they were noticeably more specific to the epoched behaviour, especially in the case of wake and SWS minimal and maximal behaviour. Unlike the sleep-scored clustering, there was no significant different between hippocampal and cortical clustering. Motion scored clusters were generally less specific than sleep-scored clusters.

Table 3.2.3: Behavioural Specificity in Motion Scored Clusters. Calinski-Harabasz evaluation was used in cluster selection for this analysis. n = 11 (2 subjects).

		Gross Behaviour								
		Wake			SWS			REM		
Region	Value	M	SF	BM	M	SF	BM	M	SF	BM
CTX	Mean	10.3	46.5	18.9	67.5	41.4	0.8	61.1	33.9	2.2
	SEM	2.9	3.1	2.0	10.9	10.3	0.2	9.0	8.9	0.3
HIP	Mean	9.3	43.5	19.7	51.0	30.6	1.5	57.1	36.2	2.5
	SEM	2.9	4.1	2.3	10.9	10.8	0.6	7.5	7.6	0.5
		Epoch Behaviour								
		Wake			SWS			REM		
Region	Value	M	SF	BM	M	SF	BM	M	SF	BM
CTX	Mean	32.1	88.1	93.3	80.7	74.0	56.0	60.6	24.0	19.9
	SEM	11.3	3.1	1.7	7.8	9.3	8.7	8.8	9.9	8.7
HIP	Mean	39.0	87.6	92.0	78.4	66.8	59.3	46.1	26.4	7.8
	SEM	13.3	2.9	2.2	8.3	9.8	10.1	8.7	8.9	3.0

To supplement the results in Table 3.4.3, which outlined the distribution of sleep states into single clusters, Table 3.2.4 shows the distribution of the predominant behaviour from each epoch in the motion scored clusters. The gross behaviour total was

calculated from the total behaviour across all brain states and the epoch behaviour total was limited to the total behaviour in a single brain state.

The "wake" cluster contains the vast majority of maximal movement and the movement from the sleep scored wake state. The "REM" cluster contained comparable amounts of total behaviour to the sleep-scored clusters, which were themselves highly sensitive to the epoched behaviour. The "SWS" clustering was less sensitive, but contained a comparable amount of total behaviour and epoched behaviour to the sleep-scored data. In contrast with the sleep-scored datasets, the hippocampal and cortical clustering were not significantly more or less sensitive than the other with the exception of wake motionlessness ($p<0.05$).

K-means clustering of sleep-scored data is highly specific, but less sensitive while clustering of the motion scored data is highly sensitive, but less specific. Clustering of the motion scored data was sensitive to both gross and epoched behaviour.

Table 3.2.4: Behavioural Sensitivity in Motion Scored Clusters. n = 11 (2 subjects).

		Gross Behaviour								
		Wake			SWS			REM		
Region	Value	M	SF	BM	M	SF	BM	M	SF	BM
CTX	Mean	15.2	51.5	78.3	30.1	26.4	11.9	44.1	24.7	12.3
	SEM	4.9	8.2	5.5	5.2	4.9	3.9	6.0	4.2	3.2
HIP	Mean	9.7	44.3	74.2	36.4	18.2	7.2	41.7	18.3	11.0
	SEM	3.9	6.8	4.4	3.2	4.1	2.0	5.6	2.9	2.8
		Epoch Behaviour								
		Wake			SWS			REM		
Region	Value	M	SF	BM	M	SF	BM	M	SF	BM
CTX	Mean	50.0	69.8	85.2	42.4	47.9	26.2	79.8	93.3	59.8
	SEM	8.6	6.8	5.4	3.5	7.2	5.8	5.0	3.9	14.3
HIP	Mean	21.5	63.8	79.0	46.0	41.4	20.0	86.2	84.9	58.8
	SEM	7.8	6.7	5.6	5.2	5.1	5.0	2.7	3.8	7.5

3.3 K-Means Clustering TAC Dependent on Sample Size

To investigate the suitability of k-means clustering as a non-arbitrary method of

sleep stage scoring, motion scored data was presented to the k-means algorithm without restriction. The same features extracted from the scored clusters were also extracted from the motion scored ones and served as a basis of comparison. In order to determine the effectiveness of k-means clustering as a non-arbitrary technique for sleep stage detection, the relative effectiveness was calculated as the agreement between motion scored clusters and sleep scored stage stages. The total accuracy (TAC; TAC = (A+B+C)/3) was an overall measure of the sensitivity, or the amount of a scored epoch found in a given clusters, and specificity, or the amount of a cluster represented by a given epoch.

First, the sensitivity of the clustering was determined. The maximum percentage of a given sleep stage contained in any motion scored cluster for each CVI was used. For the purposes of this study, the EMG-derived sleep-scored epochs were assumed to be 100% accurate for the sake of simplicity. The motion scored clustering was not subject to the same constraints as the sleep-scoring algorithm, most notably, the minimum state duration and gap. Table 3.3.1 shows the distribution of sleep stages in the motion scored clusters. Naïve clustering (n=19) was notably sensitive to REM and SWS detection as were sham and tDCS and to a lesser extent, tACS. Wake, by contrast, had the lowest agreement in any of the conditions.

Table 3.3.1: Sleep Stage Sensitivity in Motion Scored Clusters. Values give the mean percentage of a given sleep stage found in an motion scored cluster ± SEM. Baseline n = 19 (3 subjects), task = 4 (1 subject)

		Pre-Task			Post-Task		
Cond.	Region	Wake	SWS	REM	Wake	SWS	REM
Base.	CTX	63.9 ± 1.7	86.7 ± 2.7	97.7 ± 0.4		-	
	HIP	67.4 ± 1.9	69.5 ± 4.3	87.9 ± 4.0		-	
Sham	CTX	57.2 ± 8.8	60.8 ± 8.3	92.5 ± 1.1	54.8 ± 2.5	72.8 ± 8.6	80.7 ± 7.9
	HIP	48.8 ± 1.7	73.3 ± 3.4	62.3 ± 6.0	57.6 ± 2.6	67.0 ± 9.5	78.8 ± 8.3
tDCS	CTX	65.8 ± 8.8	67.5 ± 7.2	98.1 ± 1.1	69.0 ± 3.4	73.2 ± 11.6	95.6 ± 6.0
	HIP	69.4 ± 8.1	61.3 ± 16.8	98.1 ± 1.1	61.6 ± 9.7	61.2 ± 7.3	93.0 ± 14.2
tACS	CTX	57.8 ± 3.1	67.5 ± 5.6	86.2 ± 4.4	48.5 ± 1.8	65.7 ± 4.6	85.4 ± 5.8
	HIP	46.0 ± 1.5	53.6 ± 1.2	69.0 ± 2.5	56.0 ± 1.9	57.8 ± 0.9	60.7 ±2.3

Next, the cluster features of the motion scored clusters were extracted and compared to standard sleep scoring criteria in rats (Pagliardini et al., 2013; Timo-Iaria et al., 1970). SWS was defined as ≥40% of total power in the delta band and REM was defined as ≥ 40% total power in the theta band. Figure 3.3.1 shows the variable statistics of the motion scored baseline clusters.

Table 3.3.2 shows the extracted cluster statistics of the motion scored clusters. There was no interaction between task conditions and band power (two-way repeated measures ANOVA, $F=0.56$, $p=0.472$). However, there was a significant difference between the cluster statistics of the cortical and hippocampal states ($F=50.88$, $p<0.001$).

Table 3.3.2: Cluster Statistics of Motion Scored Sleep States. Values are presented as mean ± SEM unless otherwise indicated.

Cluster Statistics								
	Cortex				Hippocampus			
Features	UP	DOWN	REM	Wake	UP	DOWN	REM	Wake
Coverage (%)	18.08	20.99	6.53	40.73	17.11	21.48	20.04	27.17
SEM	0.00	0.02	0.03	0.26	0.01	0.05	0.17	0.14
Lifespan (sec)	1.54	2.15	1.20	9.96	0.98	1.14	0.85	1.51
SEM	0.08	0.05	0.08	1.24	0.01	0.04	0.02	0.06

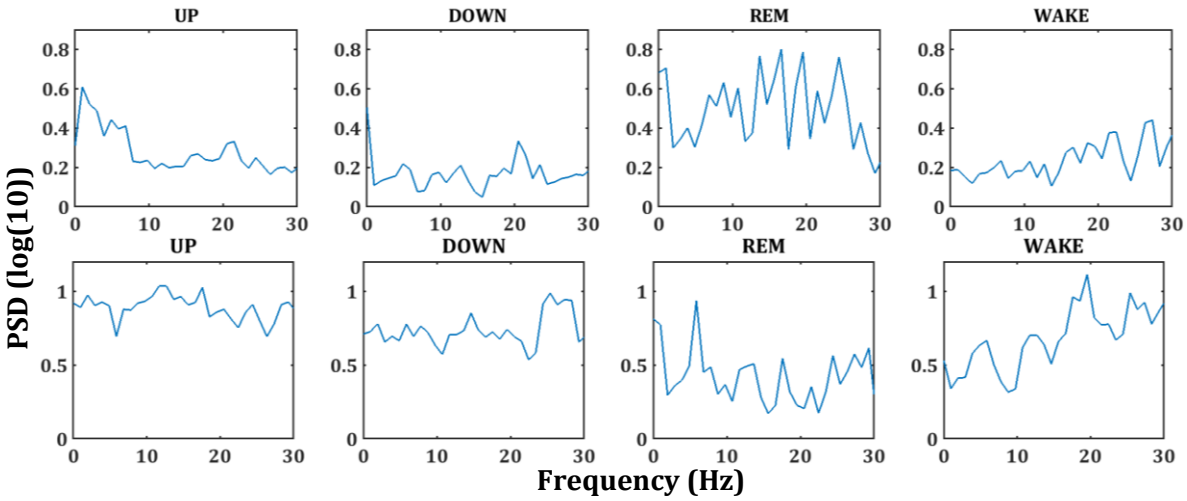

Figure 3.3.1: Absolute Spectral Power of Motion Scored Sleep States. Top: Cortex. Bottom: Hippocampus.

3.4 Coherence Sensitive to Procedural Learning Paradigm and Stimulation

To determine whether there was coherence between the primary motor cortex and the hippocampus, the magnitude-squared coherence was determined under naïve baseline and task conditions. To further clarify the relevance of the coherence, CPSD analysis was also conducted to determine the phase delay between coherent frequencies. Figure 3.4.1 shows the mean coherence and coherency in wake, SWS and REM sleep in baseline recordings and Figure S1 shows the coherence by day. SWS coherence shows limited coherence in the delta range, possibly due to competition with respiration-entrained oscillations in the same range. The peaks in the theta range in REM are consistent with the desynchronization characteristic of REM. It should be noted that unless the peaks are found in both the coherence and CPSD analyses, they can be assumed to be "noise" (See Methods Section 2.6 for further clarification).

Figure 3.4.2 shows the mean coherence in wake, SWS and REM sleep during pre-task rest and post-task rest in task conditions. There is notable coherence conservation of the theta peaks in REM across conditions. Unexpectedly, the trend in tACS SWS more

closely resembled REM than either of the other SWS conditions, potentially as a result of the disruption of SWS by the application of the stim. The low delta coherence could be due to the presence of non-hippocampal, competing delta range inputs such as respiration-entrained oscillations. The pre-task average for sham REM also had peaks in the delta range that were not present in post-task REM. Figures S2-7 shows the sham, tDCS and tACS coherence by day. Figure S9 shows the confidence interval of artifact peaks. Significant coherence supports coupling between the primary motor cortex and the hippocampus, but must be further investigated to determine whether the coherent signals are real or not i.e. non-volume conducted signals. In this study, cross power spectral density and phase delay measurements were used to that end.

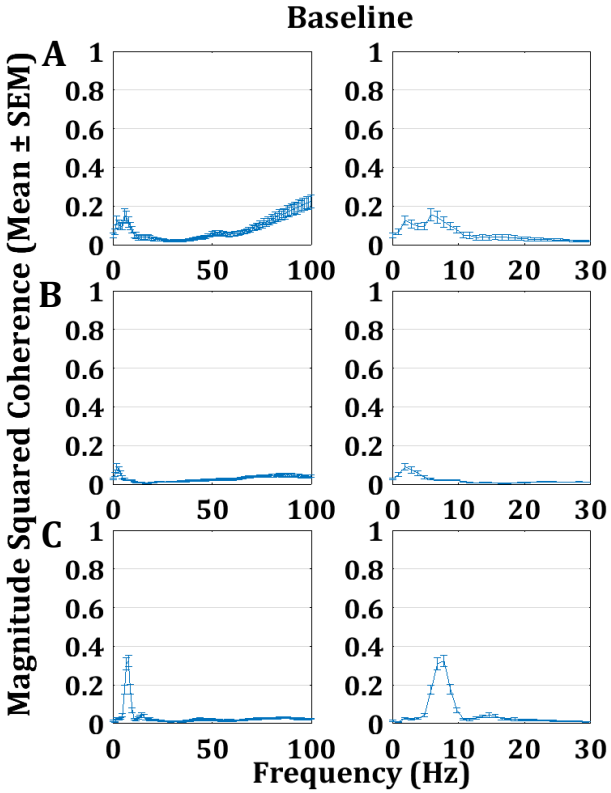

Figure 3.4.1: Mean Baseline Coherence. $C_p<0.001$ in all brain states. Frequencies above 100 Hz are significant in wake. Note the limited coherence in the delta range of SWS, the increase in theta range of REM and increase in both the delta and theta ranges of Wake. 3 subjects across a total of 19 sessions.

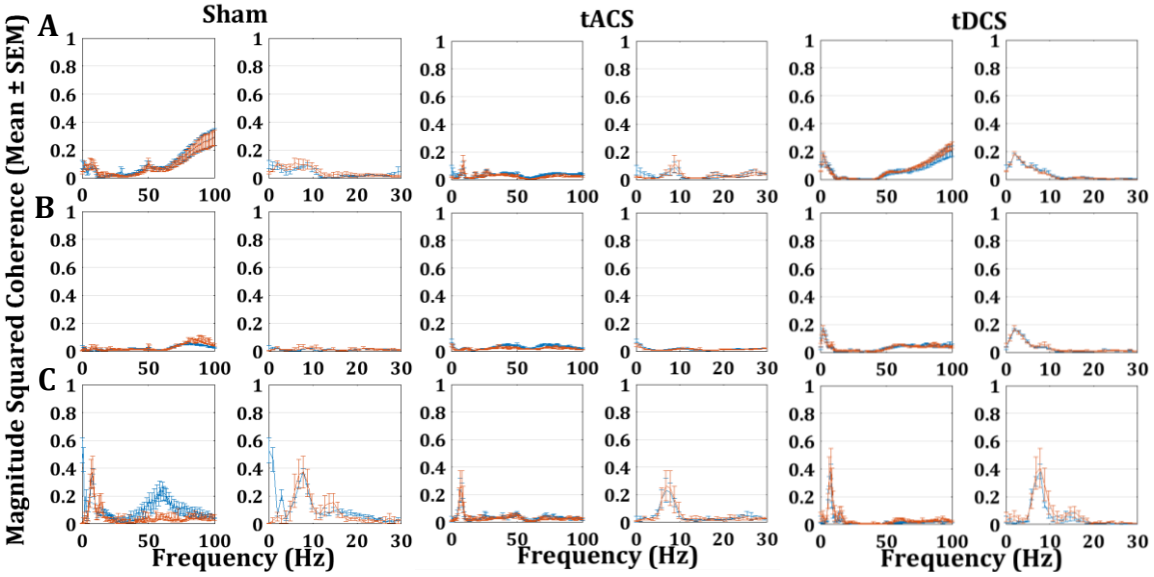

Figure 3.4.2: Mean Task Coherence. C_p<0.001 in all brain states and conditions. Blue traces and red traces indicate pre-task and post-task, respectively. A) Wake. B) SWS. C) REM. Note the significant differences between pre- and post-task sham during REM. 1 subject/condition with 4 sessions.

The CPSD gives the correlation of the cortical and hippocampal signals while maintaining phase information. Non-zero power and zero lag indicate the likely presence of a volume conducted signal. There are special cases where there can be non-zero power, zero lag signals without volume conduction (Hindrinks et al., 2016), but they are ignored for the purposes of this study as the detection methods require a different experimental design. Positive phase delay indicates the phase of cortical signal preceded the hippocampal one and negative phase delay indicates the inverse. In stationary signals, this also serves as a measure of causality between input and output signals, but in this case, the signals are non-stationary and the positive and negative phase delay should not be considered an indication of the causal relationship between the signals. A significance threshold (coherency) was applied to all phase delay calculations to minimize noise.

Figure 3.4.3 shows the CPSD and phase delay in degrees of the cortical and hippocampal signals during the baseline recordings. In REM, the division of low (4-7 Hz) and high theta (7-12 Hz) between different degrees of phase lag is of especial interest as this would imply that different ranges within theta originate in different structures. There is positive phase delay from the high spindle range through the low and high gamma range. The CPSD and phase delay plots also reveal that some of the high coherence peaks were likely volume conducted signals, leaving only a few remaining in SWS and REM. None of the ripple range peaks remain, only frequencies under 50 Hz in the case of SWS and 100 Hz in the case of REM. The high coherence in the majority of wake frequencies also had zero phase lag with the exception of the theta range, implying a large amount of volume conduction during wake with only lower frequencies coupling between the primary motor cortex and the hippocampus.

Figure 3.4.4 and Figure 3.4.5 show the CPSD and the phase delay, respectively, of the cortical and hippocampal signals under task conditions. Unexpectedly, the phase delay for the pre-task tDCS REM theta range was paralleled in post-task, appearing inverted compared to the post-task range in sham and tACS. This contrasts with the suppression of coherence observed in tACS SWS, which otherwise mirrors baseline. To a lesser extent, pre-task across all three brain states resembled baseline in tDCS and sham. The phase delay in tDCS and tACS wake is consistent with baseline coherency and is of further interest as it would seem contrary to the desynchronization expected during wakefulness.

Thus, learning-dependent changes to real i.e. non-volume conducted coherent signals between the primary motor cortex and hippocampus appear inverted by tDCS and

suppressed by tACS delivered during their respective sleep stages through visual inspection.

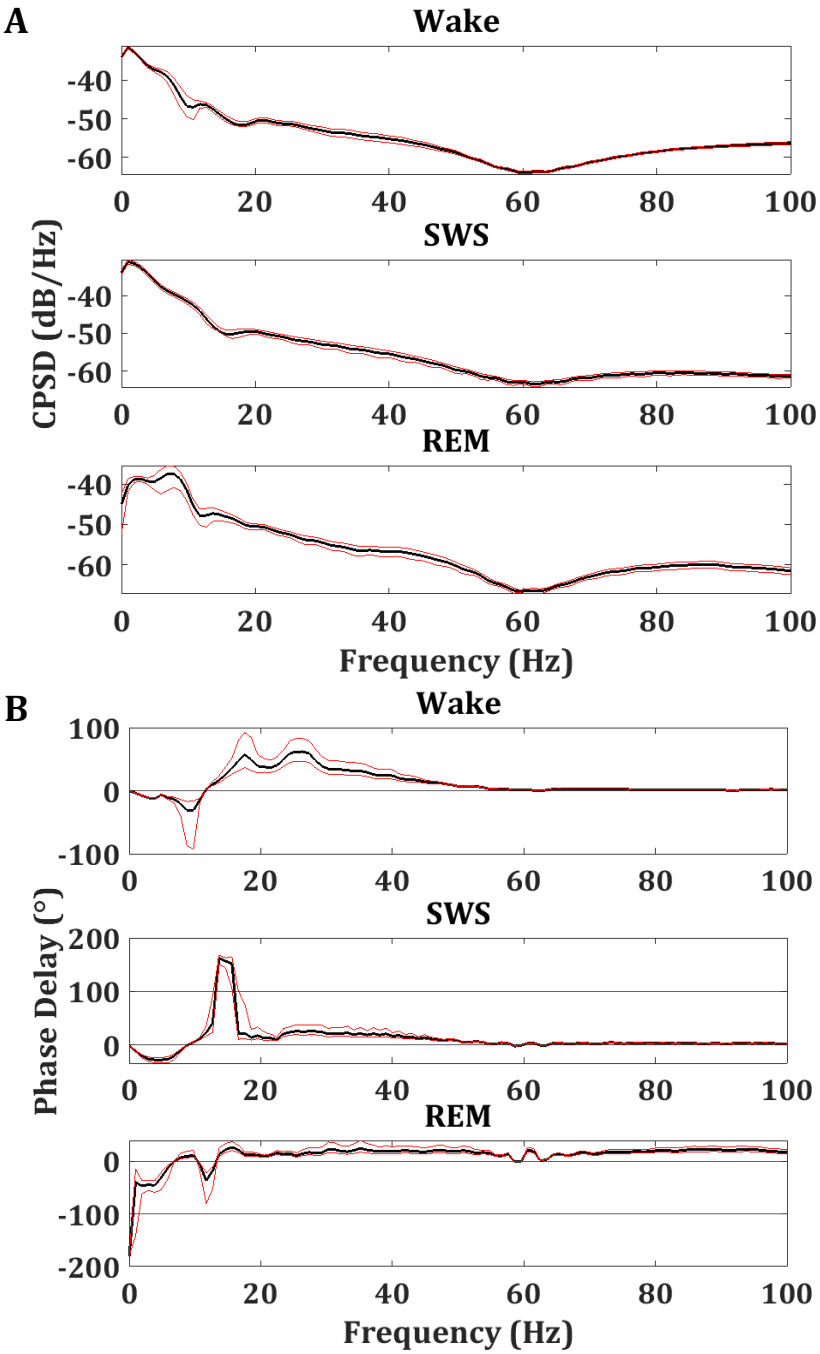

Figure 3.4.3: Baseline Mean Cross Power Spectral Density and Phase. Black and red traces give the mean and SEM, respectively. A) Cross power spectral density of wake, SWS and REM sleep in M1 and HIP. Deflections from the trend indicate shared cross power contribution to the power of that frequency. B) Cross spectrum phase of signals from M1 and HIP. 19 total sessions from 3 subjects

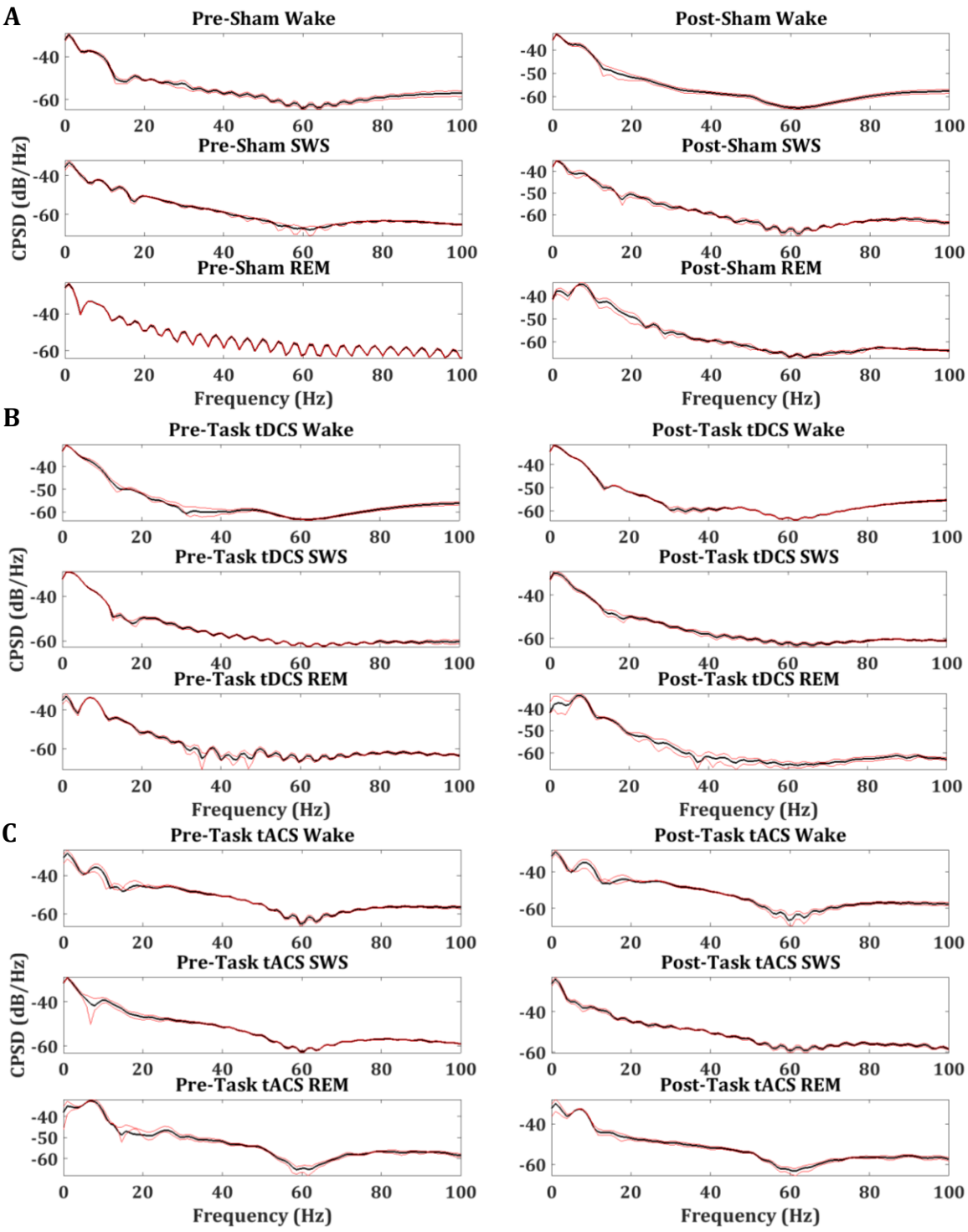

Figure 3.4.4: Task Cross Power Spectral Density. Black and red traces give the mean and SEM, respectively. Deflections from the trend indicate frequencies where both M1 and HIP contributed to power. Note that the deflections mirror the peaks in the magnitude-squared coherence. A) Sham pre- and post-task. B) tDCS pre- and post-task. C) tACS pre- and post-task. 1 subject/condition with 4 sessions each.

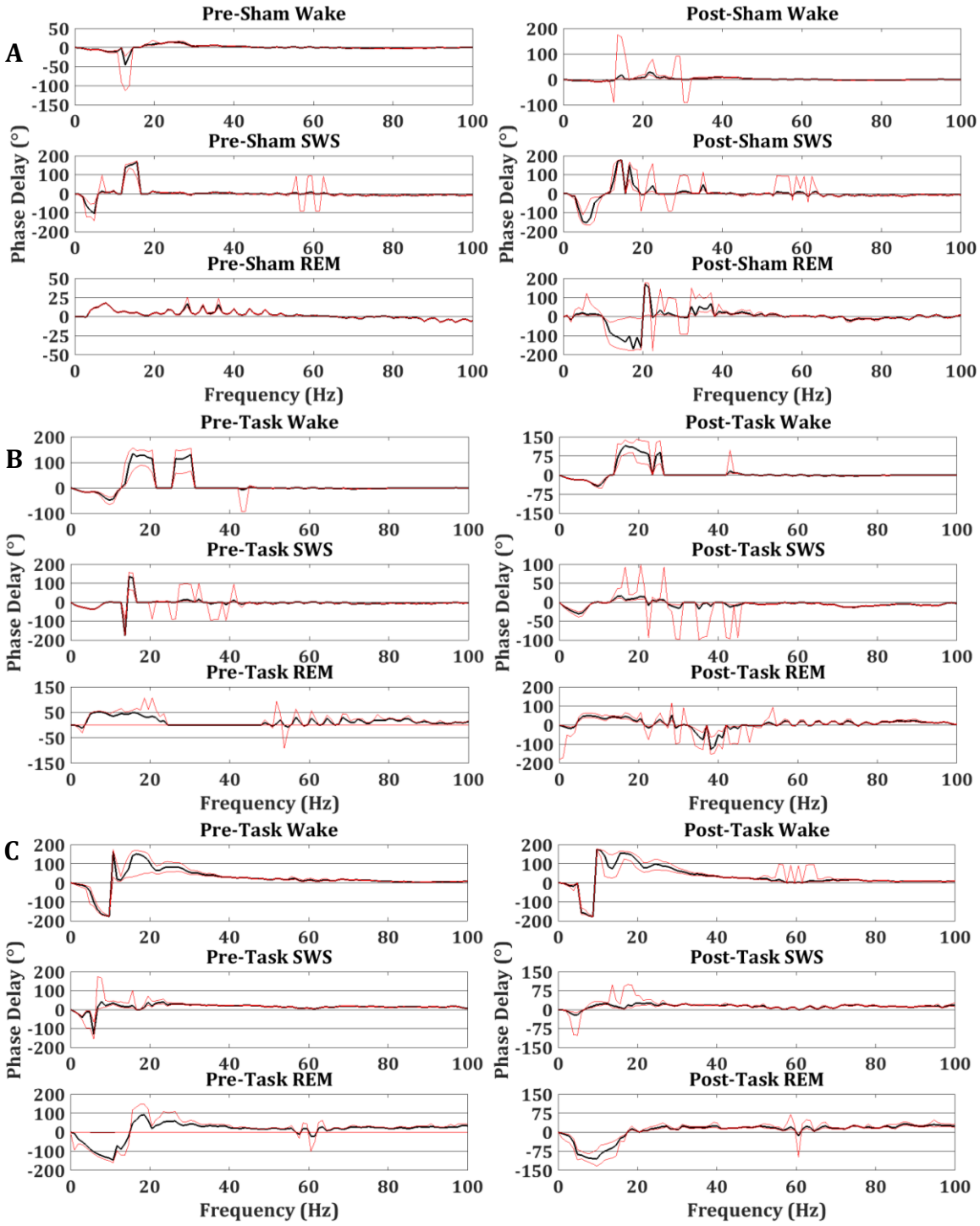

Figure 3.4.5: Task Cross Spectrum Phase. Black and red traces give the mean and SEM, respectively. Zero phase delay (degrees) and CPSD ≠ 0 indicate the signal was volume conducted. Positive values indicate the phase of the M1 signal was ahead of the HIP one and negatives values the inverse. A significance threshold (C_p<0.001) was applied prior to averaging. Left: Pre-task. Right: Post-task. A) Sham B) tDCS. C) tACS. 1 subject/condition with 4 sessions each.

3.5 Cross-Frequency Coupling Strength Increases Inter-Regionally

With the presence of strong coherency established i.e. coupling of the same frequency, further investigation of frequency-domain coupling was undertaken, specifically cross-frequency coupling. Functionally significant CFC has been observed in numerous hippocampal-dependent processes (See Section 1.4), but its presence in hippocampal-independent processes is less known. In phase-amplitude coupling, a fast frequency (f_A) is entrained by a slow frequency (f_P) such that its amplitude changes according to the slow frequency. The tPAC algorithm gives a measure of the strength of the coupling between f_A and f_P. Figure 3.5.1 shows representative hippocampal tPAC and IRtPAC comodulograms and the intersection of peak frequency for amplitude and peak frequency for phase (red circle). Only the maximum peak in each epoch was analyzed in this study.

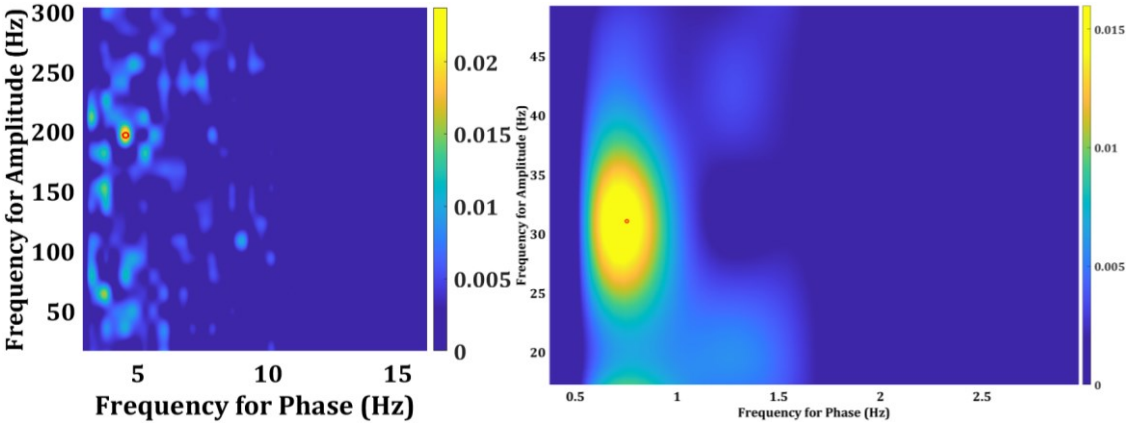

Figure 3.5.1: Representative tPAC and IRtPAC Comodulograms. The hippocampal tPAC comodulogram is on the left and the IRtPAC on the right. Red circle indicates intersection of peak frequency for phase and amplitude. The figure was smoothed through interpolation.

Datasets were segmented such that the lowest frequency for phase of interest (0.5 Hz<f_P) could complete at least 4 cycles within the epoch before being analysed with tPAC and averaged. Because of the segmentation, the minimum n (the number of segments) for each session was 50 for wake, 50 for SWS and 20 for REM. Table 3.5.1

outlines the phase-amplitude coupling in baseline and task wake. Despite a stable frequency for phase and coupling strength across conditions, the frequency for amplitude changed in both sham and tACS conditions. In sham, it increased from the beta range to high gamma while in tACS, the inverse was observed. The coupling of delta range (~1 Hz) oscillations with beta (~20 Hz) and gamma range (90 – 300 Hz) is consistent with respiration-entrained oscillations (RR). These oscillations are temporally and spatially ubiquitous and can only be distinguished from other slow wave oscillations by measuring the respiration rate. The coupling in the hippocampus was insensitive to the learning paradigm during wake. Thus, there is a stimulus- and learning-insensitive CFC relationship (delta-beta and delta-gamma) during wake in both the hippocampus and the primary motor cortex.

Table 3.5.1: Wake Phase-Amplitude Coupling.

		Cortex			Hippocampus		
Condition	Time	PAC (x10^{-3})	f_P	f_A	PAC (x10^{-3})	f_P	f_A
Base	Pre	18.0	1.0	277.9	11.4	1.0	20.0
Sham	Pre	17.0	1.3	20.0	15.6	1.0	20.0
	Post	16.4	1.0	241.1	14.5	1.3	20.0
tDCS	Pre	15.8	1.0	20.0	15.6	1.3	152.6
	Post	15.9	1.0	20.0	17.2	1.0	152.6
tACS	Pre	16.1	1.0	255.8	12.4	1.5	93.7
	Post	20.3	1.0	20.0	11.7	1.5	93.7

Table 3.5.2 shows the phase-amplitude coupling in baseline and task SWS. Notable differences in the hippocampal frequency for amplitude were observed. In both tACS and sham, it increased from beta and low gamma to high gamma. The PAC strength in cortical tACS nearly doubled between pre- and post-task sessions while PAC strength in sham and tDCS decreased. SWS coupling strength was inversely sensitive to learning and tACS, unlike the frequency for amplitude changes. Delta-beta coupling in the cortex during SWS appears to strengthen following tACS, but weaken during sham

and tDCS while in the hippocampus, the strongest CFC relationship in sham and tACS conditions changed from delta-beta and delta-low gamma to delta-high gamma.

Table 3.5.2: SWS Phase-Amplitude Coupling.

		Cortex			Hippocampus		
Condition	Time	PAC (x10^{-3})	f_P	f_A	PAC (x10^{-3})	f_P	f_A
Base	Pre	21.7	1.0	20.0	16.4	1.0	130.5
Sham	Pre	23.4	1.3	20.0	17.9	1.0	20.0
	Post	19.2	1.3	20.0	18.3	1.5	123.2
tDCS	Pre	18.2	1.0	20.0	27.7	1.0	137.9
	Post	14.2	1.0	20.0	23.0	1.3	137.9
tACS	Pre	18.4	1.0	20.0	13.0	1.5	49.5
	Post	32.8	1.0	20.0	11.5	1.3	108.4

Table 3.5.3 shows the phase-amplitude coupling in baseline and task in REM. Note that the coupling strength is significantly lower during REM than in either wake or SWS. Unlike in the other brain states, the frequency for phase was not conserved between the cortex and the hippocampus, mirroring the division in the theta range coherence. The hippocampal frequency for phase remained at a consistently high theta frequency while the cortical frequencies varied between low and high theta across sessions. The frequency for amplitude slowed in both the hippocampus and cortex in post-task tDCS. The cortical frequency for amplitude in cortical sham increased from low gamma to high gamma. While the PAC strength increased in both sham and tDCS, it decreased in tACS. Phase-amplitude coupling within the cortex and hippocampus was sensitive to learning and both stim conditions during their respective delivery periods. The learning-associated changes often contrasted with the stim-associated ones.

Table 3.5.3: REM Phase-Amplitude Coupling.

		Cortex			Hippocampus		
Condition	Time	PAC (x10^{-3})	f_P	f_A	PAC (x10^{-3})	f_P	f_A
Base	Pre	3.8	3.8	64.2	4.4	7.3	20.0
Sham	Pre	4.8	3.8	64.2	3.5	7.1	137.9
	Post	6.8	4.5	285.3	5.0	6.8	137.9
tDCS	Pre	4.9	3.8	152.6	8.0	7.1	79.0
	Post	6.0	3.8	137.9	8.7	7.3	20.0
tACS	Pre	6.6	4.0	152.6	11.4	6.3	49.5
	Post	5.7	3.8	152.6	7.0	7.1	49.5

Throughout the tPAC analysis, similar frequencies for phase and amplitude were observed in the hippocampus and cortex. To determine whether these coincidental similarities reflected phase-amplitude coupling between the two regions, IRtPAC analysis was carried out.

Table 3.5.4 shows the IRtPAC results for baseline and task conditions in all brain states. The most striking difference was the increase in coupling strength in all three brain states across all conditions compared to tPAC. In wake, coupling strength increased in sham and decreased in tDCS and tACS post-task. The frequency for amplitude increased in both sham and tDCS to high gamma while in decreased modestly in tACS. In SWS, the coupling strength decreased in sham and tACS although only modestly in the case of tACS, while it increased in tDCS. The frequency for amplitude in sham increased from the beta range to the low gamma range. This low gamma range was maintained in both pre- and post-task tDCS while in tACS, the frequency for amplitude increased within the high gamma range. In REM, the coupling strength increased in sham and tACS while decreasing in tDCS. The frequency for phase increased to high theta in sham, but not tDCS or tACS post-task. The frequency for amplitude slowed in both sham and tDCS, but to different extents.

IRtPAC coupling strength in both stim conditions tended to decrease during the sleep stage of the respective delivery periods. IRtPAC and tPAC coupling strength was responsive to both stim conditions as well as the learning paradigm.

Stimulation appeared to disrupt inter-regional coupling between the primary motor cortex and the hippocampus compared to stim. The PAC strength was elevated following learning in all three conditions compared to baseline. In connection with the coherence and CPSD analysis, not only does there appear to be endogenous coupling between the primary motor cortex and hippocampus, it also affected by a procedural learning task and electrical manipulation.

Table 3.5.4: Inter-Regional Phase-Amplitude Coupling.

		Wake			SWS			REM		
Cond.	Time	PAC ($x10^{-3}$)	f_P	f_A	PAC ($x10^{-3}$)	f_P	f_A	PAC ($x10^{-3}$)	f_P	f_A
Base	Pre	21.2	1.0	241.1	24.3	1.0	211.6	8.9	3.8	64.2
Sham	Pre	35.1	1.0	108.4	45.6	1.3	20.0	10.4	4.0	71.6
	Post	40.3	0.8	182.1	36.4	0.8	49.5	14.9	6.8	20
tDCS	Pre	34.6	1.3	20.0	24.7	0.8	49.5	16.0	3.8	123.2
	Post	26.7	1.3	182.1	26.3	1.3	49.5	9.9	3.8	93.7
tACS	Pre	41.7	1.0	152.6	35.8	1.3	241.1	12.4	3.8	49.5
	Post	36.0	1.3	123.2	34.6	1.0	255.8	16.0	3.8	211.6

4. Discussion

This project examined the relative effectiveness of an unsupervised algorithm in the detection of global and local microstates in the primary motor cortex of male rats and the effect of a procedural learning paradigm on these microstates under sham and stim conditions as described by the outcomes of several semi- and non-arbitrary techniques. K-means clustering revealed several stable and transient microstates in SWS and REM as well as the presence of cortical SWS-like REM states. Clustering of motion scored data exceeded the threshold for successful sleep stage detection with high concordance with automated sleep scoring. There was significant coherence verified by CPSD found in the theta and gamma ranges of tDCS and sham conditions that was sensitive to the procedural learning task. Clustering was sensitive and specific to behaviour. Calinski-Harabasz was the most behaviourally relevant in both scored and motion scored clustering. Together, these results support several global and local microstates within SWS and REM sleep in the primary motor cortex that are sensitive to procedural learning and suggest a window for consolidation of memory.

These findings support the presence of local and global LFP microstates, implicating them in procedural learning, and their detection through PCA and k-means clustering as non-arbitrary techniques. Clustering is relatively sensitive and specific to sleep states in motion scored data. Coherence, tPAC and IRtPAC are responsive to procedural-learning and transcranial stimulation. The persistence of these states under other conditions and the extent of their physiological roles requires further research.

4.1 Clustering as an Effective Technique in Microstate Detection

Mean clustering classes supported three SWS divisions, two REM divisions and

two SWS-like REM states in the cortex. In this study, data-driven estimates of the clusters/microstates were used to explain the data rather than a priori selection although both are accepted in the literature (Tibshirani & Walther, 2005; Pascual-Marqui et al., 1995; Khanna, et al., 2014). Three SWS states were detected (LOW, UP, DOWN), which was consistent with the recent LFP and spiking studies (Miyawaki et al., 2017; Logothetis et al., 2012). LOW states often follow REM periods and precede periods of massive activations of association and primary cortical regions and potentially mediate a privileged interaction state or procedural memory consolidation between the hippocampus and cortex by silencing extraneous subcortical output centres (Miyawaki et al., 2017; Logothetis et al., 2012). The detection of cortical SWS-like REM states also supports recent findings of microstates within REM and the lack of homogeneity within both SWS and REM sleep in rodents. The absence of the two cortical SWS-like REM clusters following learning strongly suggest a learning-dependent local brain state in the primary motor cortex during natural sleep. The recovery of this microstate following pre-task administration of the tDCS could represent a change in learning dynamics. A comparison of task performance with and without intervention and the presence or absence of these microstates would serve to clarify this relationship. For example, modulation of these microstates before or after a task could influence acquisition or later retrieval. This has a number of implications for the underlying networks and the associated cognitive functions, especially with respect to memory consolidation. The presence of these states at baseline, but not following learning is suggestive of a shift between a global brain state dominated or strongly regulated by the hippocampus following learning, but that is sufficiently diminished outside of that to allow for

neocortical disconnect.

4.2 Clustering as an Effective Classifier of Sleep Stages

K-means clustering-mediated sleep detection was sensitive and specific to each brain state, especially REM, and extracted cluster features were consistent with the standard rat sleep phase metrics (Zhang & Wu, 2018; Timo-Iaria et al., 1970; Miyawaki et al., 2017). Overall performance based on the total accuracy reported in the literature for sleep detection methods is usually between 70% and 95% (Charbonnier et al., 2011). With a baseline TAC between 74.9% and 82.8%, the clustering implemented here was comparable with automated sleep scoring ratings and has the potential for improved performance with additional information passed to the algorithm including: EMG data and minimum durations for sleep periods. It is clear that the algorithm is sensitive to the sample size and case should be taken in implementation. However, there is such a wide variety of automatic sleep detection methods that comparisons of only TAC are difficult and do not reflect the reliability or convenience of the methodology (Charbonnier et al., 2011; Libourel et al., 2015). Many methods have for automatic sleep stage classification have been developed involving different techniques (Kassiri et al., 2017). However, these methods are often complex and require knowledge and expertise in advanced computational modelling, making them inaccessible (Zhang & Wu, 2018). The quality of expert manual scoring depends on individual experience and fatigue in addition to the time-consuming nature of the task. K-means clustering is becoming increasingly popular across a wide variety of analytical fields as its methodology is more accessible to the non-expert analyst and the flexibility of the datasets it can be used with. The method

presented here is a sensitive and specific non-arbitrary alternative to both manual scoring and automated scoring derived from arbitrary frequency boundaries.

4.3 Coherence Sensitivity to Procedural Learning and Transcranial Stimulation

Coherence was found to be sensitive to both the learning paradigm and tDCS and tACS stimulation. While procedural learning and tDCS seemed to increase coherence, tACS appeared to suppress it. The coherence in the SWS delta range was not especially high, likely due to the presence of overlapping respiration-entrained oscillations. During deep sleep, the respiration cycle is less than 1.5 Hz (Lockmann et al., 2016) and can thus be distinguished from theta oscillations, but not delta oscillations. It is important to note that the respiration-entrained oscillations are not artifacts of muscle activity or electrode movement (Tort et al., 2018). While the motor cortex and hippocampus respond preferentially to theta oscillations over RR in REM and exploratory wake, RR are a globally-detected phenomenon ranging between 1 Hz and 14-15 Hz and without monitoring respiration are impossible to differentiate from other physiological signals (Tort et al., 2018). The coherent theta signal in REM was expected, but the apparent division of low theta and high theta is of especial interest. This result supports both the existence of finer divisions of frequency bands representing potential microstates, especially pREM and tREM, and the presence of endogenous theta band coupling between the primary motor cortex and the hippocampus (Jing et al., 2016; Wehrle et al., 2007). Theta band coupling has been implicated in a wide variety of neuropathological states, cognitive functions and behaviour in both humans and animals (Goutagny et al., 2013; Reinhart, 2017; Zhang et al., 2016). Coherence estimates were verified by CPSD analysis, which accurately identifies volume conduction effects beyond the margins of

activated neuronal substrates, but has a slight bias against higher frequencies such that it increasingly underestimates coherence in proportion to the frequency (Kajikawa & Schroeder, 2011). These results support coherent theta and respiration-coupled delta, which have been implicated in connecting distant brain regions and mediation of memory networks.

4.4 Behavioral Segregation by Clustering

K-means clustering had behavioural relevance with respect to both scored and unscored datasets. The behaviour contained at the vertices of the distribution were highly specific, but not especially sensitive, which is consistent with these clusters containing uncontaminated primary behaviours i.e. sniffing without any other movement, locomotion and complete motionlessness. The proportion of motionlessness during REM was expected given REM sleep is characterised by low muscle tone despite being only ~20% of the total sleep duration and would thus contain a disproportionate amount of motionlessness given its relative brevity. The ratio of sniffing to motionlessness in SWS was unexpected as sniffing is conventionally regarded as an active, investigatory behaviour typically indicative of arousal (Seelke & Blumberg, 2004). However, the ubiquity of sniffing during both wakefulness and rest is consistent with the literature (Seelke & Blumberg, 2004). Regardless, the behaviour classified as sniffing in this study was not limited to exploratory sniffing and likely contained respiration changes and myoclonic twitching as a limitation of the low-resolution video recordings used for behaviour scoring. As a result, both sniffing and motionlessness were likely contaminated with off-target behaviour. Still, both scored and unscored behaviour were within reasonable bounds of minimal/no movement as expected of sleep. The first two principal

components also described behaviourally relevant aspects of the explained variance. The first principal component largely defined the degree of movement, which explained the greatest variability of the data, while the second principal component described the separation of complete motionlessness from non-motionlessness. Thus, PCA is a suitable method of dimensionally reducing datasets without loss of information. Together with higher resolution videos, PCA and k-means clustering would likely have stronger sensitivity and specificity.

4.5 Cross-Frequency Coupling Relevance to Task and Stimulation Conditions

Cross-frequency coupling was inversely sensitive to the procedural learning paradigm and both tDCS and tACS. The coupling strength and frequency for amplitude were the most directly affected. There was consistent delta-beta and delta-gamma coupling during wake and SWS in both baseline and task sessions, which was consistent the significant coherence at those frequencies. Delta-gamma coupling is both region and brain state-specific and robustly correlated with theta or RR oscillations (Zhong et al., 2017). Unexpectedly, gamma and ripple range coupling was found in the cortex during SWS. However, ripple, gamma, high gamma and ultra-high gamma (200 – 800 Hz) have been observed during sleep in primary motor cortex of rodents (Averkin et al., 2016; Hasenstaub et al., 2005; Kandel & Buzsáki, 1997). While cortical gamma and ripple range coupling could be the result of volume-conducted hippocampal ripples, given the presence of gamma range peaks in the CPSD analyses and the CPSD bias against higher frequencies, it is more likely that this coupling is the result of real cortical signals. Simultaneous oscillatory activity is characteristic of the cortical network activation and has been reported as instrumental in several higher-order cognitive processes including

post-task success and reward (Buzsáki & Draguhn, 2004; McBain & Fisahn, 2001; Salinas & Sejnowski, 2001; Singer & Gray, 1995; Steriade, 2000; van der Meer & Redish, 2009).

4.6 Relative Effectiveness of Cluster Validity Indices

With respect to behaviour, Calinski-Harabasz outperformed both Davies-Bouldin and Silhouette in terms of relative effectiveness. There are roughly three tiers of statistically distinct CVIs where CVIs within a tier are not statistically different from a peer in overall performance, but can vary greatly when given particular types of data (Arbelaitz et al., 2013; Hämäläinen et al., 2017). CH, DB and SH were all tier one CVIs, but there is no reliable a priori test of the effectiveness of a CVI with respect to a given dataset, so best practice supports selecting multiple CVIs and repeating the analysis with each. The k-means++ algorithm requires more iterations with noisy datasets than other clustering algorithms, but handles increases in dimensionality better than other clustering methods, especially when used in conjunction with CH (Hämäläinen et al., 2017). This is ideal for the complex data generated by EEG and other physiological recordings. However, it can also struggle to differentiate small subclusters near larger ones such as the marked differences in the durations of SWS and REM sleep. These characteristics could lead to the a priori assumption that k-means++ clustering and CH would be unsuitable for sleep state detection. However, k-means++ exceeded the threshold of successful sleep detection, which while contrary to expectations, underlines the lack of clear a priori criteria for CVI selection. This study supports the best practice of selecting multiple CVIs from a tier and examining the resulting clusters.

4.7 Limitations

The limitations of this study must also be acknowledged. First, there is the effect of the low number of subjects between conditions. There was only one animal undergoing each condition in the task sessions, so there is the possibility that the animals could be outliers. As a result, it is difficult to isolate the source of an effect during task conditions. While differences between pre- and post-task results were observed in the sham animal, the animals under stim conditions frequently also had differences between pre- and post-task. As such, there are two assumptions that can be made which affect the interpretation of these results: First, the results are sensitive to the learning paradigm. Thus, either a) the animals are insensitive to one or more stim conditions, so the differences from the sham trial are due to between-subject variability, or b) the animals are sensitive to the one or more stim conditions, so the differences from the sham trial are due to the interaction of stim and learning. Second, the results are insensitive to the learning paradigm and thus the differences are either between-subject variability or the results are sensitive to one or more of the stim conditions. Ideally, three or more animals would undergo the same condition to control for this ambiguity. There is the additional constraint of limited behavioural videos. As a result, task performance could not be assessed and automated sleep scoring could not be verified, limiting the degree of clustering accuracy. What videos were available were not taken with this analysis in mind and thus, were occasionally of poor quality with a limited view of the animal, so there is the potential for misclassified behaviour. It must also be acknowledged that sleep scoring is not a precise discipline regardless of whether it is automated or carried out manually. It is not unusual for even expert scoring to vary by as much as 10%. As such, there is the

possibility that the proposed local brain states are artifacts of misattributed SWS as REM. Second, there is the possibility that the scoring criteria was overly generous in its gap allowance resulting in clusters that only contain the interruptions to the sleep state rather than true microstates. This is unlikely for two reasons. First, the average duration of these cortical clusters is beyond the limits imposed by the scoring criteria and second, brief interruptions to otherwise steady states are far more frequent than appears to be contained in these clusters. Finally, the study design and data collection resulted in inconsistent recording lengths within and between conditions. Within baseline, recording lengths could vary by up to three hours and the start of the post-task sleep recording varied between immediately after the task to up to an hour later. Many post-task changes are found in the first thirty minutes of post-task sleep and would have dissipated entirely in some cases (Eschenko et al., 2008). However, the differences between roughly two hours of uninterrupted sleep and approximately hour-long sleep sessions interrupted by handling and a task should not be underestimated. Ideally, baseline recordings should have been divided into two sleep sessions with the handling by the researcher and placement in the test chamber. Additionally, animals would also be recorded from across the same days in order to allow for proper comparisons. There are also certain considerations for clustering that should encourage caution when evaluating the results of clustering algorithms. First, without a known output which would establish an endpoint, clustering will carry on until convergence, regardless of meaningfulness. A common convergence problem arises when each data point becomes a cluster with perfect, but meaningless separation. A way around this is by evaluating the clusters with a CVI. However, there is a remarkable number of CVIs all with various level accessibility and

meaningfulness without reliable a priori tests for suitability between datasets and evaluation criteria, sorting through them quickly becomes a headache. The field often uses subjective post hoc determinations of usefulness with few methods of validating the results. Validation usually amounts to using synthetic datasets which may or may not be representative of the real data in question or reshuffled data, a process beyond the processing power of the operating system used for this paper.

4.8 Future Directions

Aside from reproducing this study to overcome the various limitations outlined above, this study presents several new questions to be answered. First, the nature of the task may influence whether the associated cortical area is more or less concurrent with the global brain state and to differing extents. In this study, a motor learning task was utilized and the motor cortex investigated, but the presentation of a visual task could affect these outcomes. This leads to a line of questioning regarding whether certain cortical areas are more flexible when it comes to reliably entering the global brain state and whether tasks that rely on those areas can affect adherence to global or local brain states.

Second, given the nature of this motor task paradigm, laterality could be a factor in these effects. This paradigm was undertaken in a freely behaving rodent, which would naturally limit measuring the degree to which ipsilateral and contralateral motor behaviours were expressed. However, the question remains as to whether the contralateral motor cortex would adhere to either the global brain state or a local state found in the corresponding ipsilateral cortex. This remains a question in both naïve and task-dependent states.

Finally, there is a question of whether other techniques could complement those used in this study and clarify underlying mechanisms of action. LFP recordings in conjunction with behavioural data have given the gross outline of a difference in function. To get a finer picture, other techniques such as single-unit recordings would be useful in determining whether there are cellular changes in excitation or inhibition mediating the effects found here or whether these effects are mediated by a specific population or subpopulation of neurons.

5. Conclusion

These findings support the presence of local and global LFP microstates, implicating them in procedural learning, and their detection through PCA and k-means clustering as non-arbitrary techniques. Clustering is relatively sensitive and specific to sleep states in unscored data and behaviour. Coherence, tPAC and IRtPAC are responsive to procedural-learning and transcranial stimulation. The persistence of these states under other conditions and the extent of their physiological roles requires further research, especially due to the limitations imposed the dataset.

6. REFERENCES

Abhang, P. A., et al. (2016). *Introduction to EEG- and Speech-Based Emotion Recognition*. Retrieved from https://doi.org/10.1016/C2015-0-01959-1.

Albouy, G., et al. (2008). Both the hippocampus and striatum are involved in consolidation of motor sequence memory. *Neuron. 58*, 261-272.

Antony, J., W. & Schapiro, A. C. (2019). Active and effective replay: systems consolidation reconsidered again. *Nature Reviews Neurosci. 20,* 506-507.

Arbelaitz, O., et al. (2013). An extensive comparative study of cluster validity indices. *Pattern Recognit*, *46* (1), 243-256, doi:10.1016/j.patcog.2012.07.021

Arthur, D., & Vassilvitskii, S. (2007). K-means++: The Advantages of Careful Seeding, presented at SODA '07: Proceedings of the Eighteenth Annual ACM-SIAM Symposium on Discrete Algorithms, 1027–1035, New Orleans, Louisiana, January 07-09, 2007.

Averkin, R., et al. (2016). Identified Cellular Correlates of Neocortical Ripple and High-Gamma Oscillations during Spindles of Natural Sleep. *Neuron. 92* (4), 916-928.

Bandarabadi, M., et al. (2019). Dynamical modulation of theta-gamma coupling during REM sleep. *Sleep*, zsz182; doi:10.1093/sleep/zsz182

Başar, E., et al. (2001). Gamma, alpha, delta, and theta oscillations govern cognitive processes. *Int J Psychophysiol. 39* (2-3), 241-8.

Beckers, T, & Kindt, M. (2017). Memory Reconsolidation Interference as an Emerging Treatment for Emotional Disorders: Strengths, Limitations, Challenges and Opportunities. *Annu Rev Clin Psychol. 13,* 99-121.

Bishop, C. M. (2006). *Pattern Recognition and Machine Learning.* New York: Springer-Verlag.

Boyce, R., et al. (2016). Causal evidence for the role of REM sleep theta rhythm in contextual memory consolidation. *Science, 352* (6287), 812-816.

Boyce, R., et al. (2017). REM sleep and memory. *Curr Opin Neurobiol. 44*, 167-177.

Britton, J. W., et al. (2016). *Electroencephalography (EEG): An Introductory Text and Atlas of Normal and Abnormal Findings in Adults, Children, and Infants [Internet]*. Chicago: American Epilepsy Society. Retrieved from: https://www.ncbi.nlm.nih.gov/books/NBK390343/

Buzsáki, G. (1989). Two-stage model of memory trace formation: a role for "noisy" brain states. *Neuroscience. 31* (3), 551–570.

Buzsáki, G. (2015). Hippocampal sharp wave-ripple: A cognitive biomarker for episodic memory and planning. *Hippocampus. 25* (10), 1073-188.

Buzsáki, G. & Draguhn, A. (2004). Neuronal oscillations in cortical networks. *Science 304* (5679), 1926-9.

Buzsáki, G., et al. (2012). The origin of extracellular fields and currents — EEG, ECoG, LFP and spikes. *Nat Rev Neurosci. 13* (6), 407-420.

Canolty, R. & Knight, R. (2012). The functional role of cross-frequency coupling. *Trends Cogn Sci. 14* (11), 506-515.

Charbonnier, S., et al. (2011). Self-evaluated automatic classifier as a decision-support tool for sleep/wake staging. *Comput Biol Med. 41* (6), 380-9.

Churchwell, J., et al. (2010). Prefrontal and hippocampal contributions to encoding and retrieval of spatial memory. *Neurobiol Learn Mem. 93* (3), 415-421.

Clopath, C. (2012). Synaptic consolidation: an approach to long-term learning. *Cogn Neurodyn. 6* (3), 251-257.

Cole, S. R. & Voytek, B. (2017). Brain Oscillations and the Importance of Waveform Shape. *Trends Cogn Sci. 21* (2), 137-149.

Corsi-Cabrera, M., et al. (2000). EEG bands during wakefulness, slow-wave and paradoxical sleep as a result of principal component analysis in man. *Sleep. 23* (6), 738-44.

Corsi-Cabrera, M., et al. (2001). EEG bands during wakefulness, slow-wave and paradoxical sleep as a result of principal component analysis in the rat. *Sleep. 24* (4), 374-80.

D'Ambrosio, S., et al. (2019). Sleepiness as a Local Phenomenon. *Front. Neurosci. 13*, 1086.

Eberly, J.H. (2016). Correlation, coherence and context. *Laser Phys. 26* (8), 084004.

Eichenbaum, H. (2013). What H.M. taught us. *J Cogn Neurosci. 25* (1), 14-21.

Eschenko, O., et al. (2008). Sustained increase in hippocampal sharp-wave ripple activity during slow-wave sleep after learning. *Learn Mem. 15* (4), 222–228.

Fellous, J-M., et al (2004). Discovering Spike Patterns in Neuronal Responses. *J Neurosci. 24* (12), 2989-3001.

Fries, P. (2005). A mechanism for cognitive dynamics: neuronal communication through neuronal coherence. *TICS. 9* (10), 474–480. doi:10.1016/j.tics.2005.08.011. PMID 16150631

Gerber, E., et al. (2016). Non-Sinusoidal Activity Can Produce Cross-Frequency Coupling in Cortical Signals in the Absence of Functional Interaction between Neural Sources. *PLOS ONE. 11* (12), e0167351.

Gevins, A., et al. (1998). Monitoring working memory load during computer-based tasks with EEG pattern recognition methods. *Human Factors*, *40* (1), 79-91.

Guevara, M.A. & Corsi-Cabrera, M. (1996). EEG coherence or EEG correlation? *Int J Psychophysiol, 23,* 145-153.

Harvard University. (2008). Glossary. In *A resource from the Division of Sleep Medicine at Harvard Medical School, Produced in partnership with WGBH Educational Foundation*. Retrieved from http://healthysleep.med.harvard.edu/glossary/n-p

Goutagny, R., et al. (2013). Alterations in hippocampal network oscillations and theta–gamma coupling arise before Aβ overproduction in a mouse model of Alzheimer's disease. *Eur J Neurosci*, *38*, 3527-3527. doi:10.1111/ejn.12446

Gundel, A. & Wilson, G. F. (1992). Topographical changes in the ongoing EEG related to the difficulty of mental tasks. *Brain Topography, 5* (1), 17-25.

Hämäläinen, J., et al. (2017). Comparison of Internal Clustering Validation Indices for Prototype-Based Clustering. *Algorithms. 10,* 105.

Hasenstaub A., et al. (2005). Inhibitory postsynaptic potentials carry synchronized frequency information in active cortical networks. *Neuron. 47,* 423–435

Hasselmo, M. E., & Stern, C. E. (2014). Theta rhythm and the encoding and retrieval of space and time. *Neuroimage. 85* (02), 656-666.

Haumann, N. T., et al. (2019). Applying stochastic spike train theory for high-accuracy MEG/EEG. *bioRxiv*. doi: 10.1101/532879

Hindriks, R., et al. (2016). Discrepancies between Multi-Electrode LFP and CSD Phase-Patterns: A Forward Modeling Study. *Front. Neural. Circuits. 10,* 51.

Hinterberger, T., et al. (2014). Decreased electrophysiological activity represents the conscious state of emptiness in meditation. *Front. Psychol. 5*, 99.

Holm, A., et al. (2009). Estimating brain load from the EEG. *Scientific World Journal, 9*, 639-651.

Jing, W., et al. (2016). EEG Bands of Wakeful Rest, Slow-Wave and Rapid-Eye-Movement Sleep at Different Brain Areas in Rats. *Front. Comput. Neurosci. 10,* 79.

Jirsa, V. & Müller, V. (2013). *Figure 1*. Different types of the cross-frequency coupling. Adapted from Cross-frequency coupling in real and virtual brain networks. *Front Comput Neurosci. 7,* 78. Copyright 2013 Jirsa and Müller.

Johnson, L. A., et al. (2010). Stored-trace reactivation in rat prefrontal cortex is correlated with down-to-up state fluctuation density. *J Neurosci. 30* (7), 2650-2661.

Kajikawa, Y. & Schroeder, C. E. (2011). How local is the local field potential? *Neuron. 72* (5), 847-58.

Kaufmann, L. & Rousseeuw, P. (1990). *Finding Groups in Data: An Introduction to Cluster Analysis.* Hoboken, New Jersey: John Wiley & Sons, Inc.

Khanna, A., et al. (2014) Reliability of Resting-State Microstate Features in Electroencephalography. *PLoS One. 9* (12), e114163.

Kandel, A. & Buzsáki, G. (1997). Cellular-synaptic generation of sleep spindles, spike-and-wave discharges, and evoked thalamocortical responses in the neocortex of the rat. *J. Neurosci. 17,* 6783–6797.

Kaplan, D. M. (2004). *Estimating Significance Level for Coherences*. Retrieved from https://websites.pmc.ucsc.edu/~dmk/notes/cohere_signif/.

Kassiri, H., et al. (2017). Electronic sleep stage classifiers: a survey and VLSI design methodology. *IEEE Trans. Biomed. Circuits Syst., 11*, 177-188.

Käthner, I., et al. (2014). Effects of mental workload and fatigue on the P300, alpha and theta band power during operation of an ERP (P300) brain-computer interface. *Biol. Psychol., 102,* 118-129, 10.1016/j.biopsycho.2014.07.014

Kropotov, J. D., (2009). *Quantitative EEG, Event-Related Potentials and Neurotherapy.* Retrieved from doi:10.1016/B978-0-12-374512-5.X0001-1

Kropotov, J. D., (2016). *Functional Neuromarkers for Psychiatry.* Retrieved from doi: 10.1016/C2012-0-07144-X

Lee, J. & Park, S. (2005). Working memory impairments in schizophrenia: a meta-analysis. *J Abnorm Psychol*. *114* (4), 599–611.

Li, G., et al. (2017). Unified thalamic model generates multiple distinct oscillations with state-dependent entrainment by stimulation. *PLoS. Comput. Biol. 13* (10), e1005797. doi:10.1371/journal.pcbi.1005797

Libourel, P.-A., et al. (2015). Unsupervised Online Classifier in Sleep Scoring for Sleep Deprivation Studies. *Sleep. 38* (5), 815-828.

Lisman, J. & Buzsáki, G. (2008). A Neural Coding Scheme Formed by the Combined Function of Gamma and Theta Oscillations. *Schizophr. Bull. 34* (5), 974-980.

Lloyd, S. P. (1982). Least Squares Quantization in PCM. *IEEE Trans. Information Theory*. Vol. 28 (2), 129–137.

Lloyd, S., et al. (2013). Quantum algorithms for supervised and unsupervised machine learning. *arXiv.* 1307.0411v2

Lockmann, A. L. V., et al. (2016). A Respiration-Coupled Rhythm in the Rat Hippocampus Independent of Theta and Slow Oscillations. *J Neurosci. 36* (19), 5338-5352.

Lüthi, A. (2014). Sleep Spindles: Where They Come From, What They Do. *Neuroscientist. 20* (3), 243-56. doi: 10.1177/1073858413500854

Lynn, P. & Sponheim, S. R. (2016). Disturbed theta and gamma coupling as a potential mechanism for visuospatial working memory dysfunction in people with schizophrenia. *Neuropsychiatric Electrophysiology. 2*, 7.

McBain, C.J. & Fisahn, A. (2001). Interneurons unbound. *Nat. Rev. Neurosci. 2,* 11–23.

McGaugh, J. L. (2000). Memory—a century of consolidation. *Science. 287* (5451), 284-51.

Mecklinger, A., et al. (1992). Event related potentials and EEG components in a semantic memory search task. *Psychophysiology, 29* (1), 104-119.

Mitra, P. & Bokil, H. (2008). *Observed Brain Dynamics*. New York: Oxford University Press.

Miyawaki, H., et al. (2017). Low Activity Microstates During Sleep. *Sleep*. *40* (6), zsx066.

Pagliardini, S., et al. (2013). Spontaneous sleep-like brain state alternations and breathing characteristics in urethane anesthetized mice. *PLoS One. 8* (7), e70411.

Pascual-Marqui, R.D., et al (1995). Segmentation of brain electrical activity into microstates: model estimation and validation. *IEEE Trans Biomed Eng. 42* (7), 658-65.

Paxinos, G. & Watson, C. (2005). *The Rat Brain in Stereotaxic Coordinates*. (5th ed.). Burlington, VT: Elsevier Academic Press.

Peever, J. & Fuller, P. M. (2016). The biology of REM sleep. *Curr Biol. 26* (1), R34-R35.

Quillfeldt, J. A. (2019). Temporal Flexibility of Systems Consolidation and the Synaptic Occupancy/Reset Theory (SORT): Cues About the Nature of the Engram. *Front. Synaptic Neurosci. 11,* 1.

Rångtell, F. H., et al. (2017). Learning performance is linked to procedural memory consolidation across both sleep and wakefulness. *Sci. Rep. 7*, 10234.

Rasch, B. & Born, J. (2013). About sleep's role in memory. *Physiol Rev*. *93* (2), 681-766.

Reinhart, R. (2017). Disruption and rescue of interareal theta phase coupling and adaptive behavior. *PNAS*. 201710257.

Richard, T. C. & Pan, S. C. (2017). Time for considering the possibility that sleep plays no unique role in motor memory consolidation: Reply to Adi-Japha and Karni. *Psychol. Bull. 143*, 454-458.

Roohi-Azizi, M., et al. (2017). Changes of the brain's bioelectrical activity in cognition, consciousness, and some mental disorders. *Med. J. Islam Repub. Iran.* 31:53.

Salinas, E. & Sejnowski, T.J. (2001). Correlated neuronal activity and the flow of neural information. *Nat. Rev. Neurosci. 2,* 539–550.

Samiee, S. & Baillet, S. (2017). Time-resolved phase-amplitude coupling in neural oscillations. *NeuroImage. 159*, 270-279.

Schroeder, C. & Lakatos, P. (2009). Low-frequency neuronal oscillations as instruments of sensory selection. *Trends Neurosci. 32* (1), 10.

Scoville, W. B. & Milner, B. (1957). Loss of recent memory after bilateral hippocampal lesions. *J. Neurol. Neurosurg. Psychiatry. 20* (1): 11–21.

Seelke, A.M. & Blumberg, M.S. (2004). Sniffing in infant rats during sleep and wakefulness. *Behav. Neurosci. 118* (2), 267-73.

Shirvalkar, P., et al. (2010). Bidirectional changes to hippocampal theta–gamma comodulation predict memory for recent spatial episodes. *PNAS. 107* (15), 7054-7059.

Shumway, R. H. & Stoffer, D. S. (2017). *Time series analysis and its applications: with R examples (4th ed.).* Springer Texts in Statistics, Springer, Cham.

Singer, W. & Gray, C.M. (1995). Visual feature integration and the temporal correlation hypothesis. *Annu. Rev. Neurosci. 18,* 555–586.

Sirota, A. & Buzsáki, G. (2005). Interaction between neocortical and hippocampal networks via slow oscillations. *Thalamus Relat Syst*. *3* (4), 245-259.

Steriade, M. & Deschenes, M. (1984). The thalamus as a neuronal oscillator. *Brain Res Rev. 8*, 1-63.

Steriade, M. & Llinás, R. R. (1988). The functional states of the thalamus and the associated neuronal interplay. *Physiol Rev. 68*, 649-742.

Steriade, M., et al. (1993). A novel slow (< 1 Hz) oscillation of neocortical neurons in vivo: depolarizing and hyperpolarizing components. *J. Neurosci*. *13* (8), 3252-65.

Steriade, M. (2000). Corticothalamic resonance, states of vigilance and mentation. *Neuroscience. 101,* 243–276.

Tadel, F., et al. (2011). Brainstorm: A User-Friendly Application for MEG/EEG Analysis. *Comput. Intell. Neurosci. 2001*, Article ID 879716.

Tibshirani, R., & Walther, G. (2005). Cluster Validation by Prediction Strength. *J. Comput. Graph. Stat. 14,* 511–528.

Timo-Iaria, C., et al. (1970). Phases and states of sleep in the rat. *Physiol Behav. 5* (9), 1057-62.

Tort, A., et al. (2009). Theta-gamma coupling increases during the learning of item-context associations. *PNAS. 106* (49), 20942-20497.

Tort, A., et al. (2010). Measuring phase-amplitude coupling between neuronal oscillations of different frequencies. *J. Neurophysiol. 104* (2), 1195-1210.

Tort, A., et al. (2018). Respiration-Entrained Brain Rhythms Are Global but Often Overlooked. *Trends Neurosci. 41* (4), 186-197.

Ulrich, D. (2016). Sleep spindles as facilitators of memory formation and learning. *Neural Plasticity*. doi: 10.1155/2016/1796715

van der Meer, M.A.A. & Redish, D.A. (2009). Low and High Gamma Oscillations in Rat Ventral Striatum have Distinct Relationships to Behavior, Reward, and Spiking Activity on a Learned Spatial Decision Task. *Front Integr Neurosci. 3,* 9.

Varela, F., et al. (2001). The brainweb: phase synchronization and large-scale integration. *Nat. Rev. Neurosci. 2* (4), 229-39.

Vyazovskiy, V. V., et al. (2011). Local sleep in awake rats. *Nature. 472* (7344), 443-447.

Voloh, B., et al. (2015). Theta–gamma coordination between anterior cingulate and prefrontal cortex indexes correct attention shifts. *PNAS. 112* (27), 8457-8462.

Voloh, B. & Womelsdorf, T. (2016). A Role of Phase-Resetting in Coordinating Large Scale Neural Networks During Attention and Goal-Directed Behavior. *Front. Syst. Neurosci.* doi: 10.3389/fnsys.2016.00018

von Stein, A & Sarnthein, J. (2000). Different frequencies for different scales of cortical integration: from local gamma to long range alpha/theta synchronization. *Int. J. Psychophysiol*. *38* (3), 301-313.

Ward, L. M. (2003). Synchronous neural oscillations and cognitive processes. *Trends Cogn Sci. 7* (12), 553-9.

Wehrle, R., et al. (2007). Functional microstates within human REM sleep: first evidence from fMRI of a thalamocortical network specific for phasic REM periods. *Eur. J. Neurosci, 25* (3), 863-71.

Whishaw, I., et al. (1986). The contributions of motor cortex, nigrostriatal dopamine and caudate-putamen to skilled forelimb use in the rat. *Brain. 109* (Pt 5), 805-846.

Whishaw, I., et al. (1991). The impairments in reaching and the movements of compensation in rats with motor cortex lesions: an endpoint, video recording, and movement notation analysis. *Behav. Brain Res. 42*: 77-91.

Wilhelm, I., et al. (2012). Sleep-dependent consolidation of procedural motor memories in children and adults: the pre-sleep level of performance matters. *Dev. Sci. 15*, 506-515.

Yamamoto, J., et al. (2014). Successful execution of working memory linked to synchronized high-frequency gamma oscillations. *Cell. 157* (4), 845-857.

Zhang, J. & Wu, Y. (2018). Complex-valued unsupervised convolutional neural networks for sleep stage classification.

Zhang, X., et al. (2016). Impaired theta-gamma coupling in APP-deficient mice. *Sci. Rep. 6*, 21948.

Zhong, W., et al. (2017). Selective entrainment of gamma subbands by different slow network oscillations. *PNAS. 114* (17), 4519-4524.

7. APPENDIX

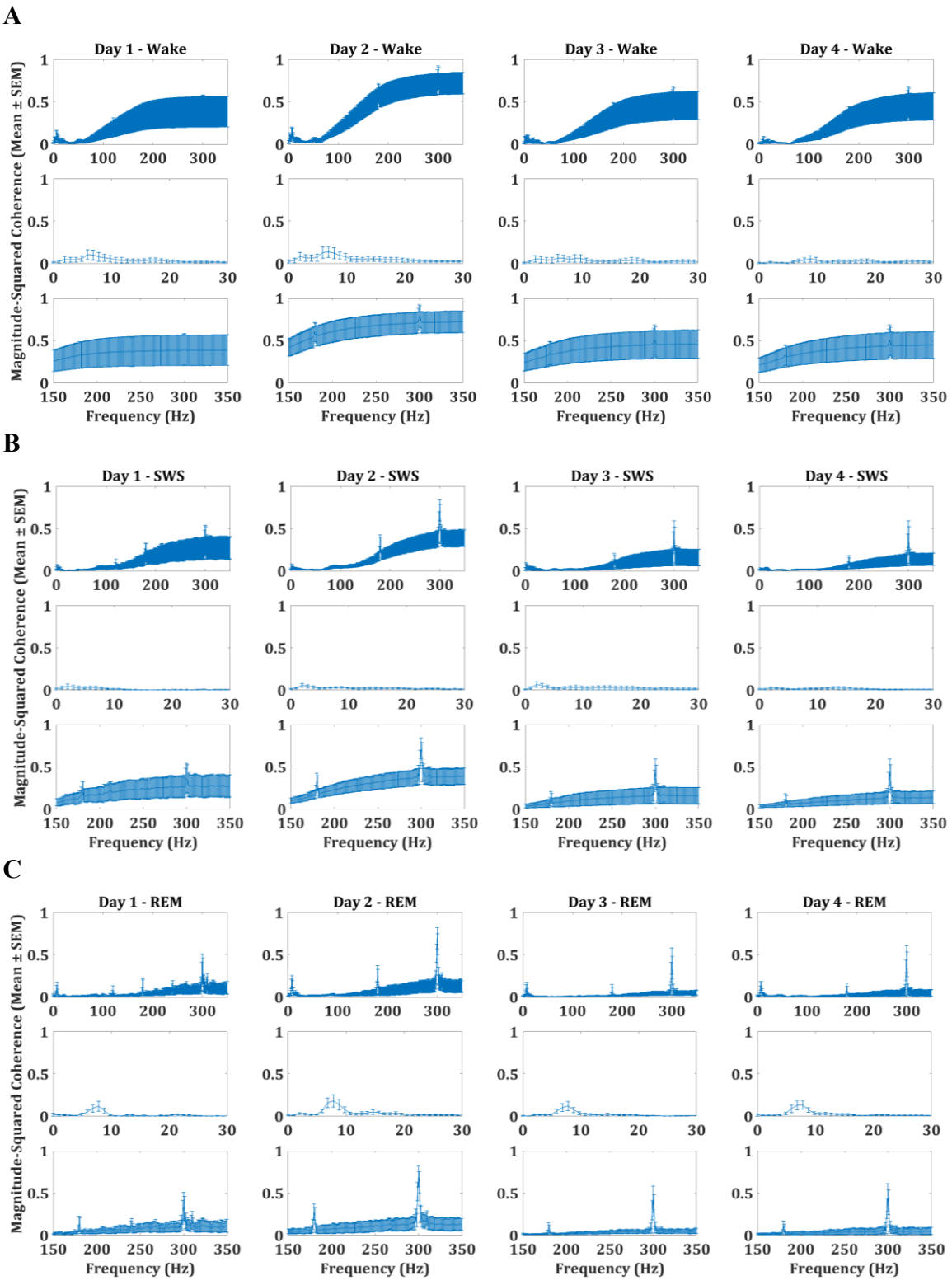

Figure S1: Baseline Coherence by Day. A) Wake. B) SWS. C) REM. Representative days selected.

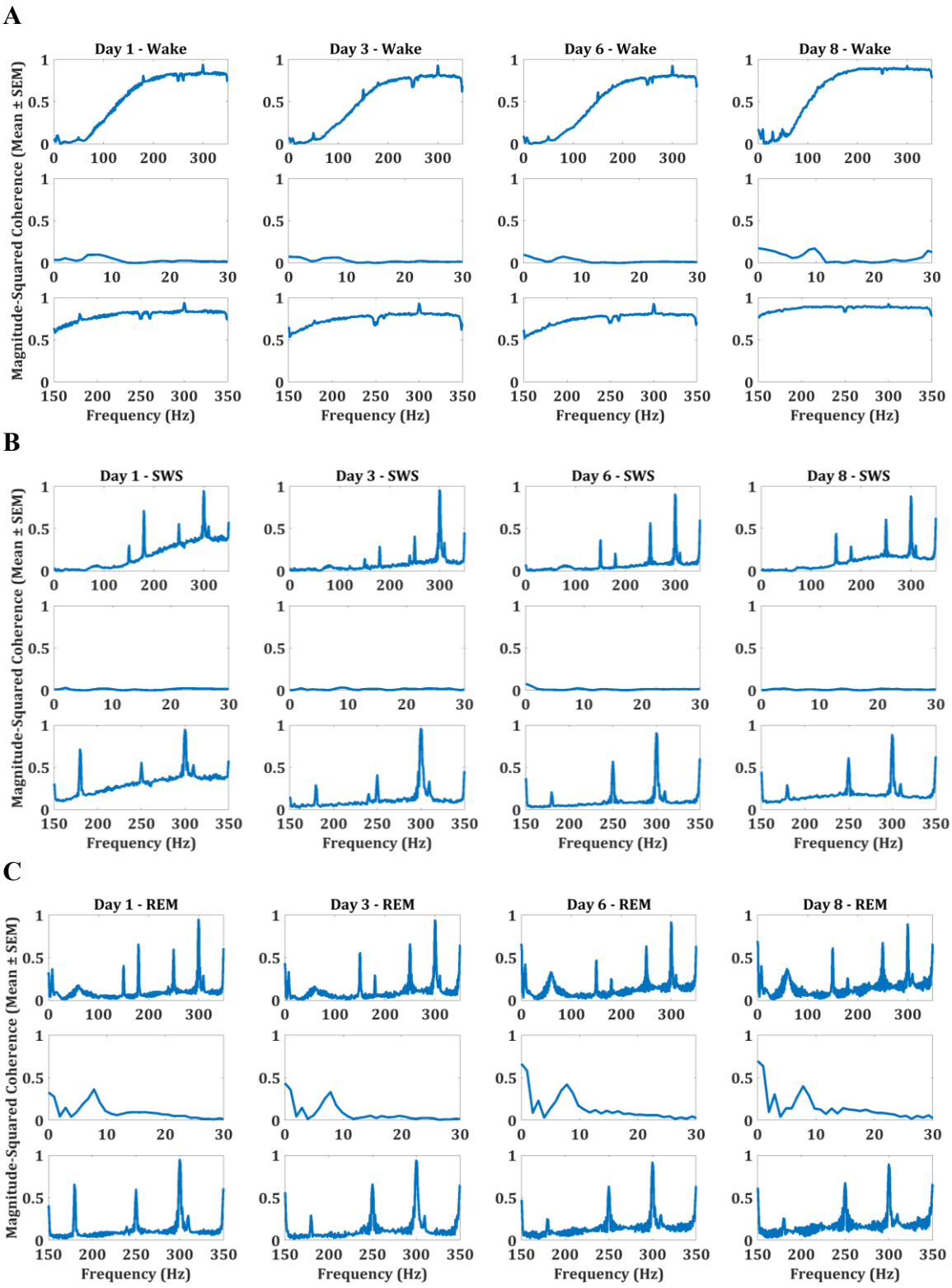

Figure S2: Pre-Task Sham Coherence by Day. A) Wake. B) SWS. C) REM.

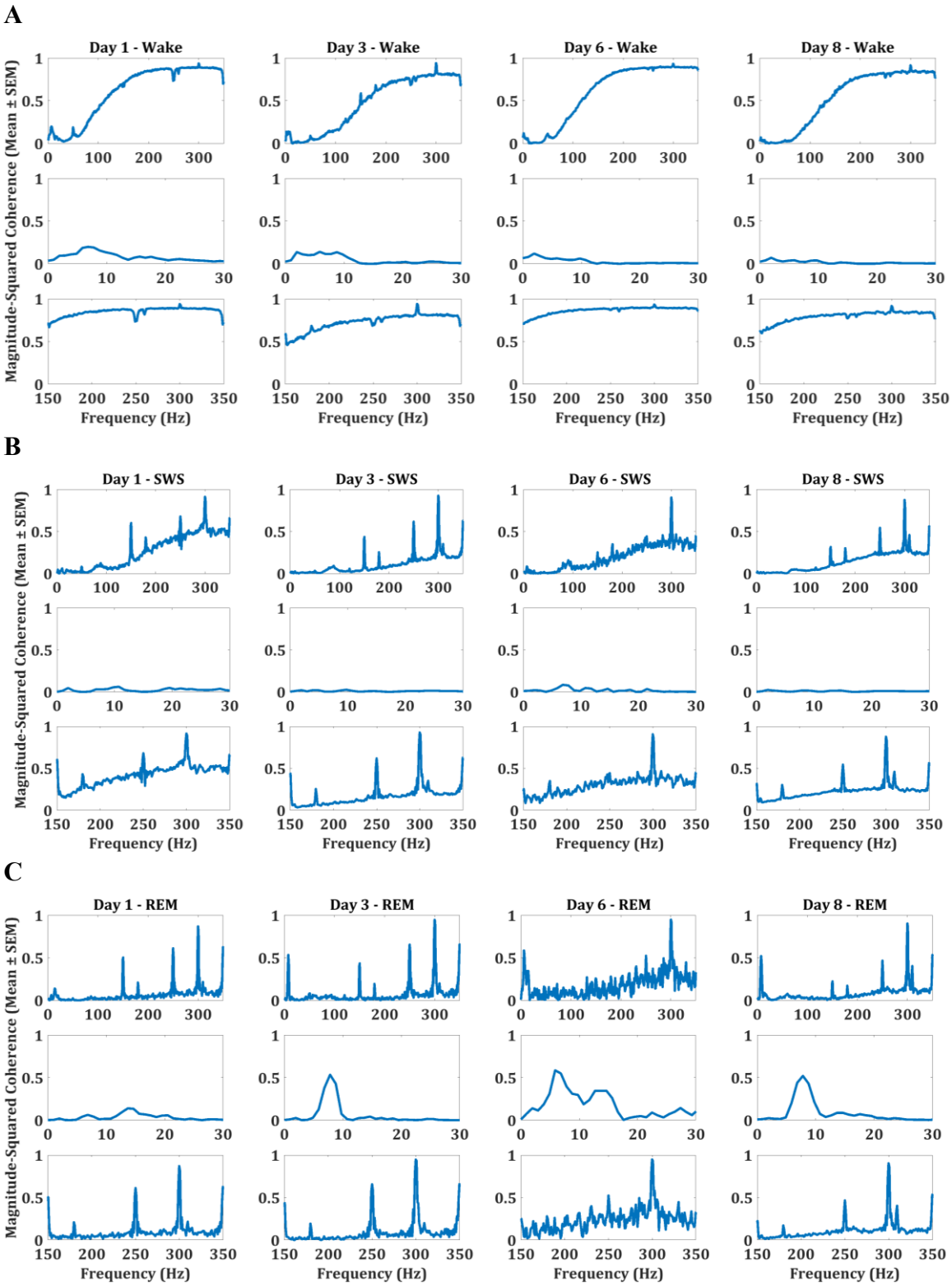

Figure S3: Post-Task Sham Coherence by Day. A) Wake. B) SWS. C) REM.

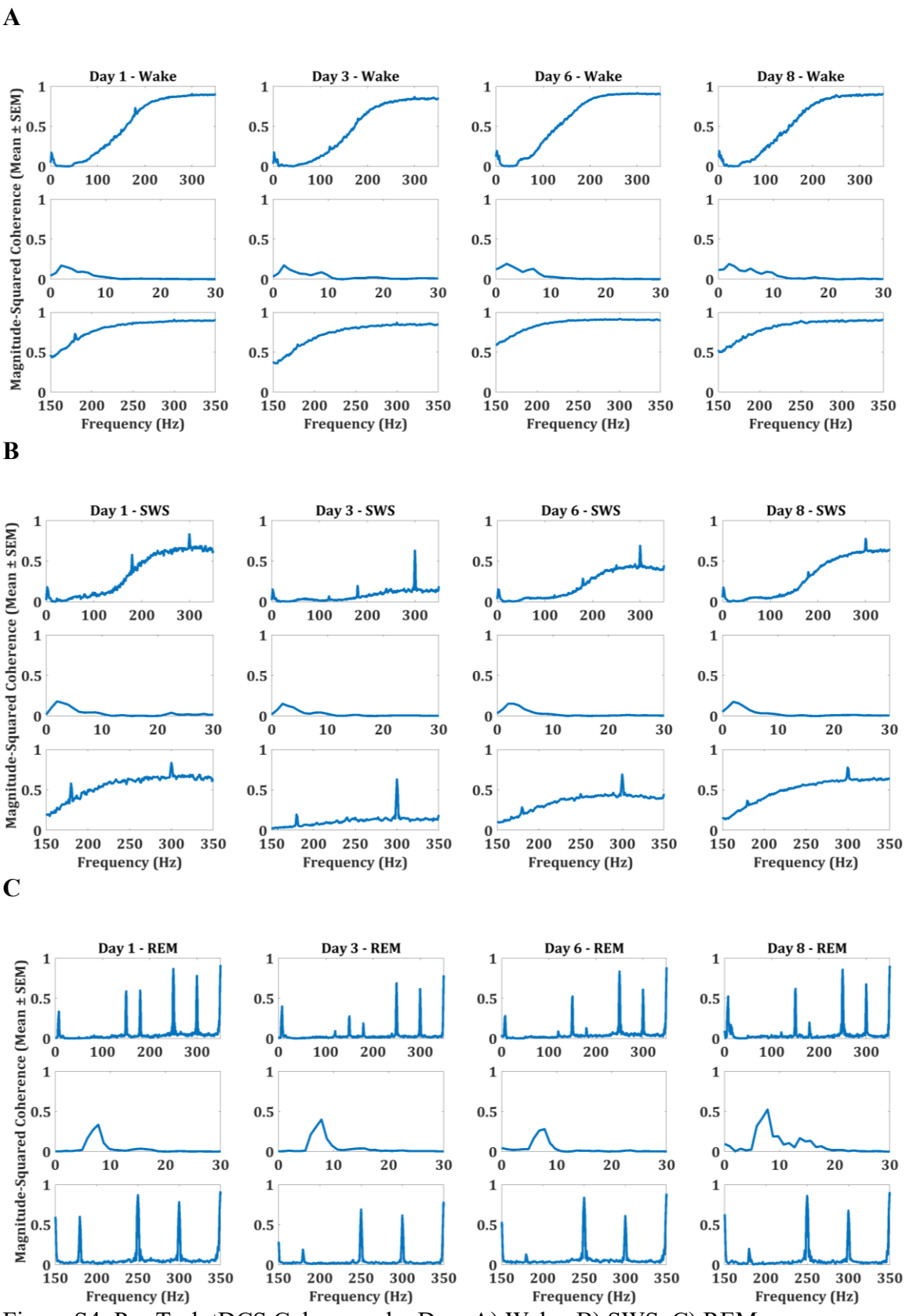

Figure S4: Pre-Task tDCS Coherence by Day. A) Wake. B) SWS. C) REM.

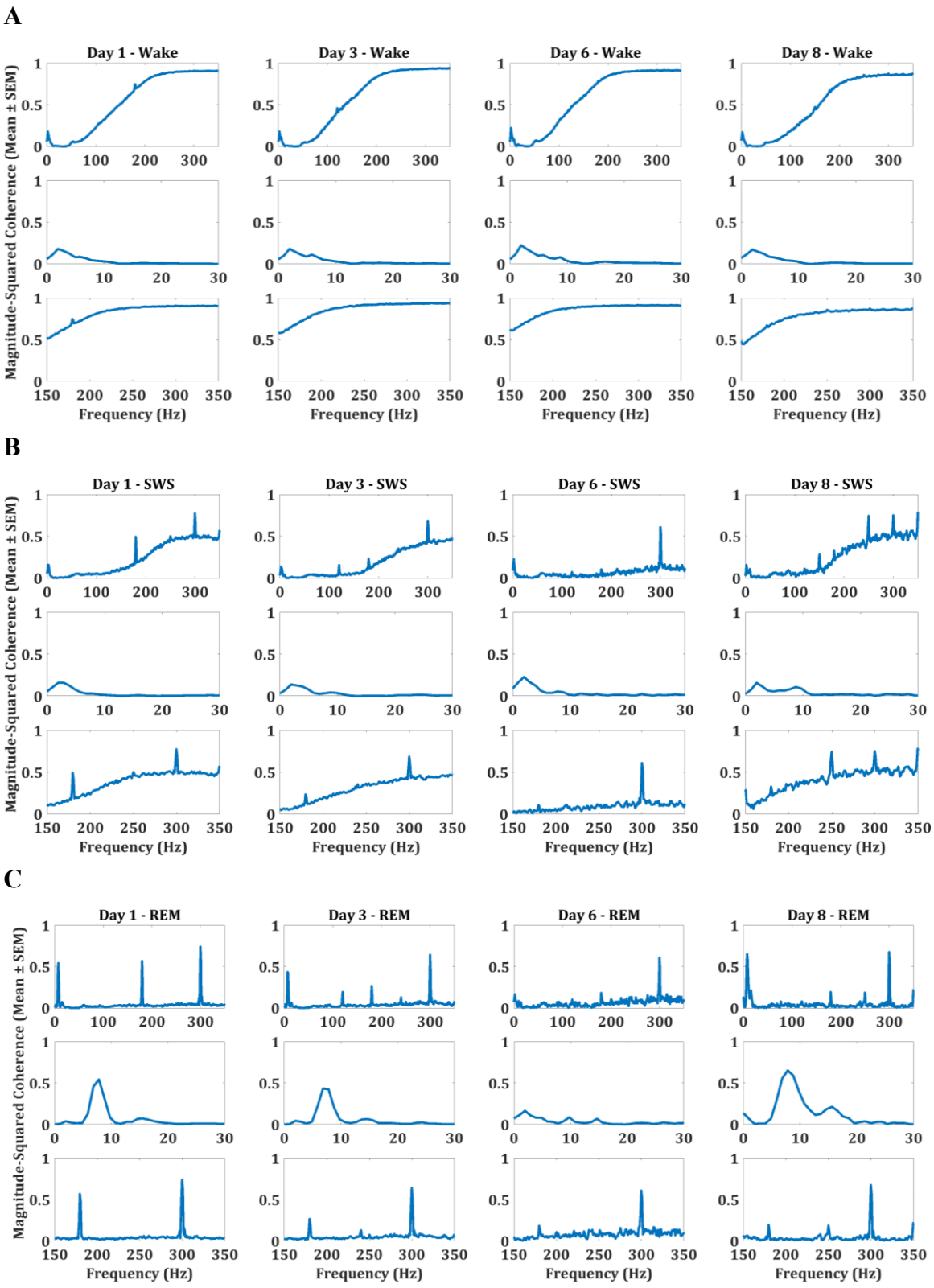

Figure S5: Post-Task tDCS Coherence by Day. A) Wake. B) SWS. C) REM.

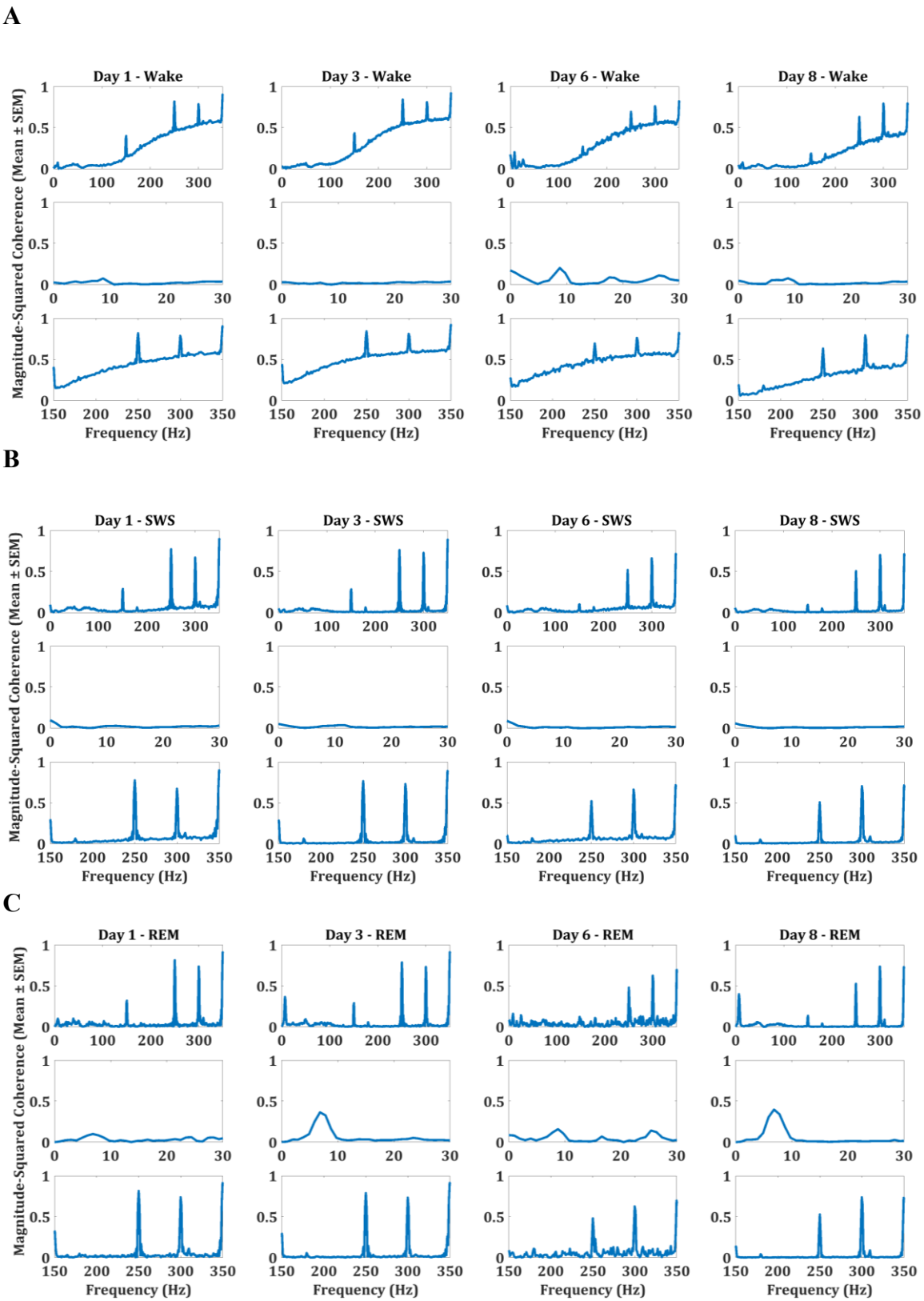

Figure S6: Pre-Task tACS Coherence by Day. A) Wake. B) SWS. C) REM.

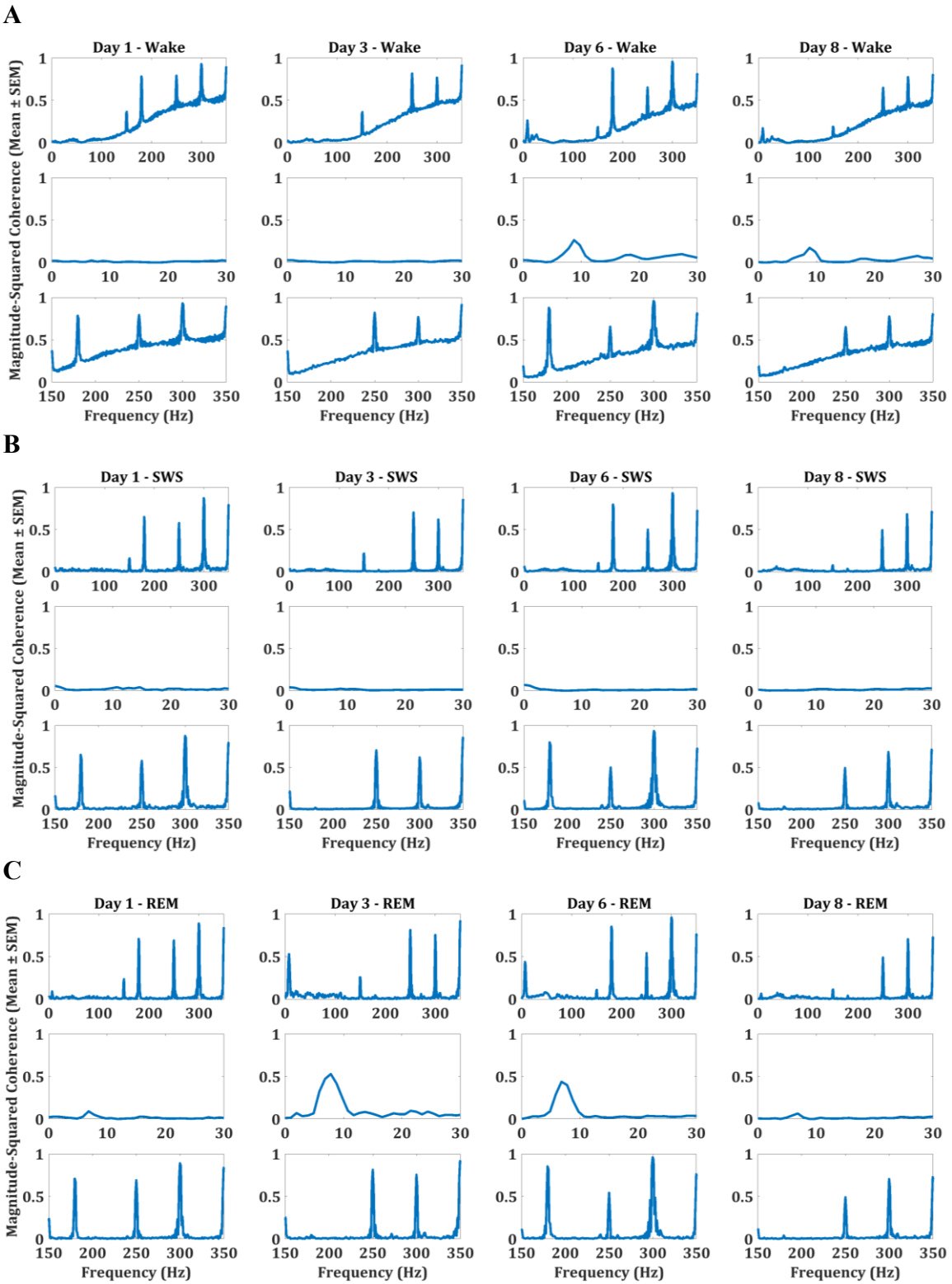

Figure S7: Post-Task tACS Coherence by Day. A) Wake. B) SWS. C) REM.

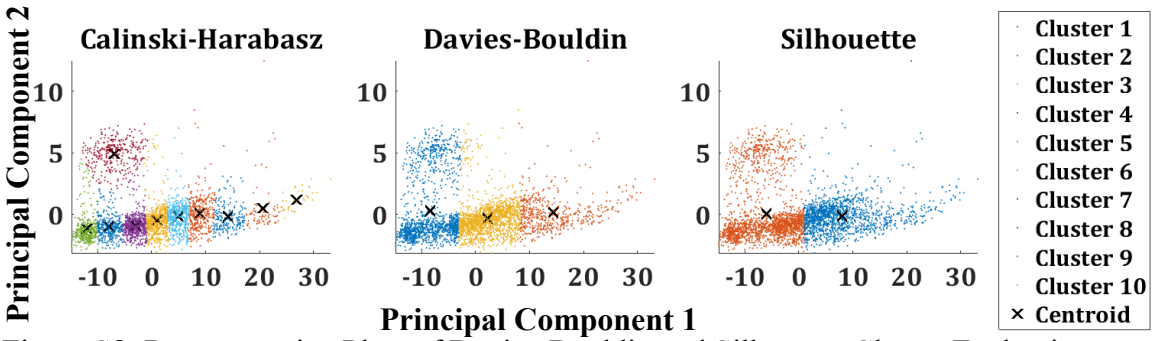

Figure S8: Representative Plots of Davies-Bouldin and Silhouette Cluster Evaluation. The motionless cluster (Cluster 7; red) was not distinguished by either Davies-Bouldin or Silhouette. The overfit exhibited in the Calinski-Harabasz validation was determined to be less detrimental to the analysis than the more accurate cluster counts in Davies-Bouldin and Silhouette with inappropriate divisions.

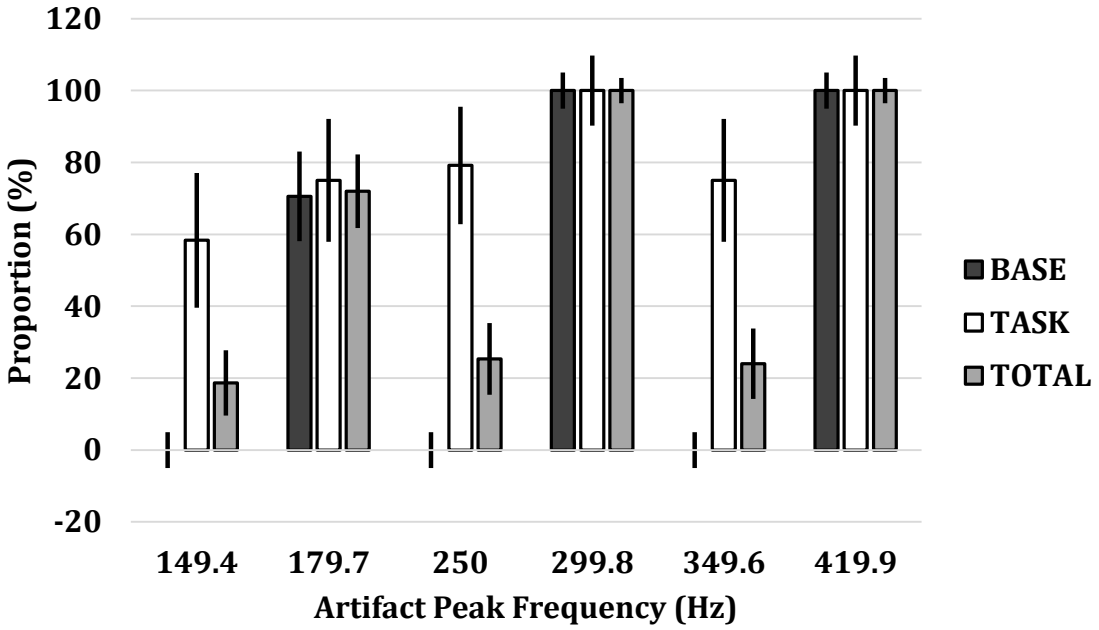

Figure S9: Artifact Peaks in Coherence. When artifact peaks were present, they were the precise frequency to a tenth of a Hertz. There was no deviation from the frequency in any condition although the strength of the peak varied. BASE = Baseline, TASK = Task, Total = Baseline and Task combined. REM, SWS and Wake were combined as the artifact peaks were present in all states. Values are given as proportion with 95% confidence interval.

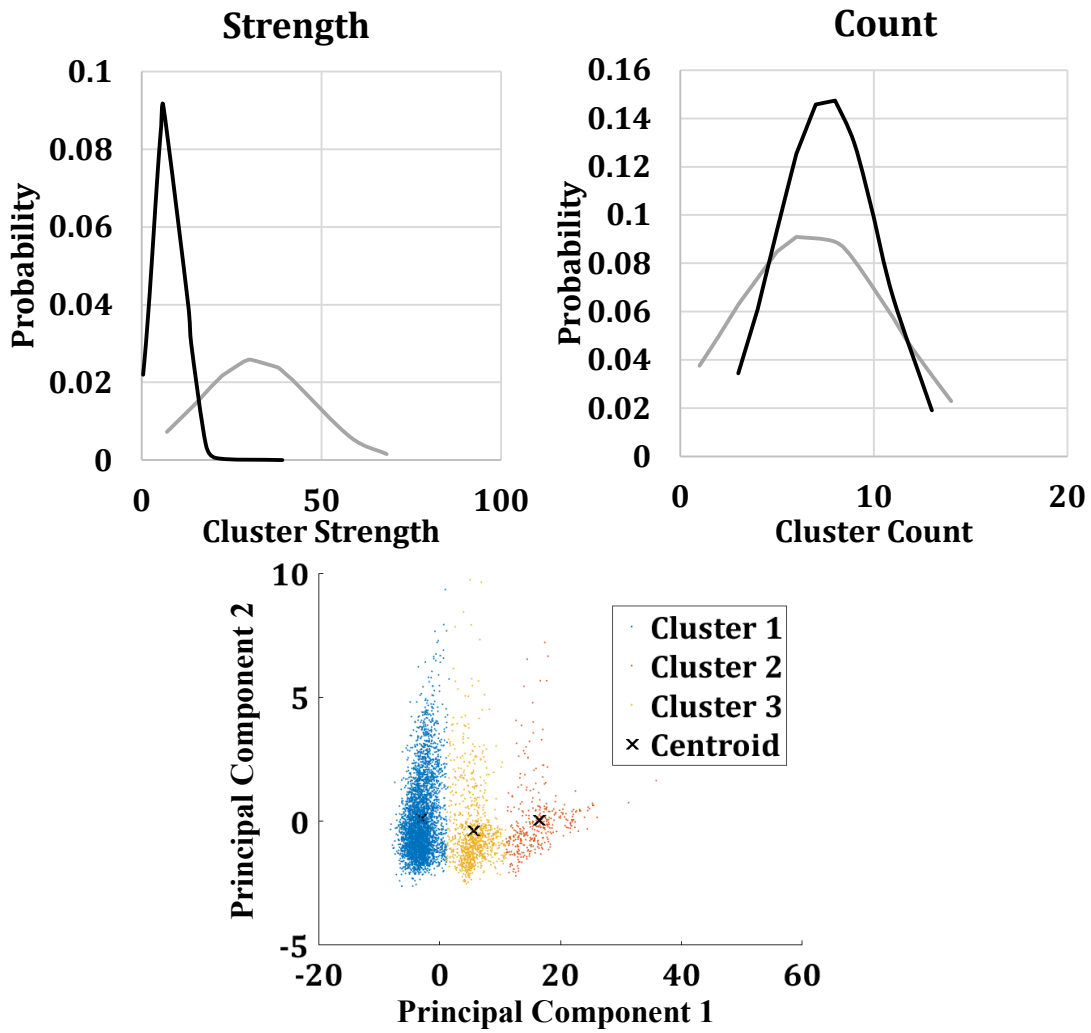

Figure S10: Representative Cluster Strength and Count Distribution. Cluster strength was calculated according to a formula by Fellous et al., 2004. There was no statistical difference between the "strongest" cluster count by this formula and those selected by Calinski-Harabasz. The strength value varied significantly (p-value < 0.05), but both the Calinski-Harabasz selected clusters and the Fellous clusters were considered strong (mean strength >2). This was consistent between all conditions and brain states. It should be noted that the strength measure varied unpredictably with "near" clusters (±1 cluster) often having a significantly different strength score whereas "near" clusters in more popular measures have values approaching the optimum. Grey = Fellous, black = Calinski-Harabasz. An example of strong Calinski-Harabasz clustering is also included (Clustering Strength 27.8).